Nucleolin rescues TDP-43 toxicity in yeast and human cell models

Caterina Peggion
Universita degli Studi di Padova Dipartimento di Scienze Biomediche
Maria Lina Massimino
Istituto di Scienze Neurologiche Consiglio Nazionale delle Ricerche
Roberto Stella
Istituto Zooprofilattico Sperimentale delle Venezie
Raissa Bortolotto
Universita degli Studi di Padova Dipartimento di Scienze Biomediche
Jessica Agostini
Universita degli Studi di Padova Dipartimento di Scienze Biomediche
Arianna Maldi
Universita degli Studi di Padova Dipartimento di Scienze Biomediche
Geppo Sartori
Universita degli Studi di Padova Dipartimento di Scienze Biomediche
Fiorella Tonello
Istituto di Scienze Neurologiche Consiglio Nazionale delle Ricerche
Alessandro Bertoli
Universita degli Studi di Padova Dipartimento di Scienze Biomediche
RAFFAELE LOPREIATO (raffaele.lopreiato@unipd.it)
Universita degli Studi di Padova https://orcid.org/0000-0003-2368-9384

Research article

Keywords: Neurodegenerative disorders, TDP-43 proteinopathies, ALS, FTD, nucleolin, misfolded proteins, yeast cells, nucleo-cytoplasmic transport, HEK293T cells

Posted Date: September 2nd, 2020

DOI: https://doi.org/10.21203/rs.3.rs-66117/v1

Abstract

Background

TDP-43 is a nuclear protein involved in pivotal processes, extensively studied for its implication in neurodegenerative disorders. TDP-43 cytosolic inclusions are a common neuropathologic hallmark in amyotrophic lateral sclerosis (ALS) and related diseases, and it is now established that TDP-43 misfolding and aggregation play a key role in their etiopathology. TDP-43 neurotoxic mechanisms are not yet clarified, but the identification of proteins able to modulate TDP-43-mediated damage may provide crucial information to unveil the molecular basis of TDP-43 proteinopathies.

Methods

Here we generated and characterized novel models of TDP-43 toxicity in the yeast *S. cerevisiae*, which were used to investigate the effect of the nucleolar protein nucleolin (NCL) on TDP-43-damaged yeast cells, by employing multiple approaches (genetics, biochemistry, microscopy). We further characterized the NCL-TDP-43 relationship in human HEK293T cells, by the combination of biochemical and microscopy-based assays.

Results

We show for the first time that NCL acts as a potent suppressor of TDP-43 toxicity in yeast models, since NCL overexpression is able to rescue TDP-43-dependent damage on cell viability and morphology, by reducing the levels of TDP-43 aggregates, thus proteostatic stress. Interestingly, data in yeast cells point to the implication of the extra-nuclear fraction of NCL in the suppressive effect. We further provide evidence that NCL co-expression alleviates the TDP-43-induced toxicity also in HEK293T cells, as indicated by the restoration of cell viability, and the diminished apoptosis activation. Importantly, biochemical and microscopy data indicate that NCL protein in human cells reduces the amount of TDP-43 inclusions. Collectively, results in HEK293T cells further support the beneficial effects of NCL on TDP-43-dependent toxicity in a more consistent pathophysiological context.

Conclusions

Altogether, data in yeast and human cell models demonstrate that NCL potently supresses the cytotoxicity caused by the TDP-43 protein, and further suggest that NCL could act by promoting the TDP-43 nuclear retention, and thus reducing the formation of cytosolic TDP-43 toxic aggregates. Pinpointing NCL as a novel player in mediating TDP-43 toxicity, experimental evidence could support NCL as promising therapeutic target in ALS and ALS-related disorders.

Background

Neurodegenerative diseases (NDs) represent a huge health problem worldwide. In most cases, the origins of neurodegeneration remain largely unknown, but it is now accepted that many of these disorders share the accumulation of misfolded protein aggregates (for which they are often referred to as proteinopathies), leading to cellular dysfunction, neuronal loss and brain damage [1]. Despite disease-associated protein aggregates in distinct NDs are different, in all cases misfolded disease-associated proteins acquire toxic functions or lose their normal function, or both [2, 3].

Among NDs, the vast majority of amyotrophic lateral sclerosis (ALS), frontotemporal dementia (FTD) and also a subset of late-onset Alzheimer's disease (AD) cases [4–8] are characterized by the presence of neuronal cytoplasmic aggregates mainly composed by a ubiquitinated and hyper-phosphorylated form of the Transactive Response DNA binding 43 kDa protein (TDP-43) [9–16]. In addition, more than 50 missense mutations in the gene encoding TDP-43 were found in 3–5% of patients with sporadic and familial ALS/FTD [17, 18], most of which (e.g., Q331K, M337V) seem to be enhancer of the intrinsic TDP-43 aggregation propensity [19, 20].

TDP-43 is a ubiquitously expressed protein, able to bind RNA/DNA by two RNA recognition motifs (RRM) along its sequence, that normally resides in the nucleus, where it plays important functions in the regulation of gene expression by modulating transcription, transcript splicing and mRNA stability, as well as microRNA biogenesis [20–22]. As a response to a variety of cellular insults, TDP-43 is also able to shuttle from the nucleus to the cytoplasm, where it is accumulated in cytosolic stress granules that have been implicated in the early stages of protein aggregation [23]. As mentioned, most of TDP-43 pathogenic mutations have been reported to promote both cytosolic translocation and the formation of insoluble aggregates, triggering cytotoxicity [18, 19].

Intriguingly, TDP-43 shares the presence of a disordered, low complexity domain C-terminal region with two other major ALS-related proteins (i.e., fused in sarcoma/translocated in liposarcoma (FUS/TLS) and C9orf72 dipeptide repeats (DPRs) [24, 25]), which is relevant to the aggregation process and is critically involved in liquid-liquid phase separation and the assembly of membrane-less organelles (e.g., stress granules), whose dysfunctions have been also implicated in the pathogenesis of ALS/FTD [26–28].

A number of NDs based on protein misfolding and aggregation, such as ALS, AD, Parkinson's disease (PD), and Hungtington's disease (HD), have been successfully modelled in the yeast *Saccharomyces cerevisiae* [29], which turned out to be highly suited to study the cellular pathways of protein aggregation and toxicity in neurodegenerative proteinopathies. In the last decade, different yeast models have been generated ectopically expressing TDP-43 at either high or low levels, mainly by the use of multicopy or centromeric plasmids, respectively [19, 30, 31]. However, such expression systems may lead to significant variations in the expression of heterologous protein because the number of plasmid copies maintained by yeast cells was scarcely controllable and may affect strain genetic stability, being the expression levels of the transgene also dependent on the used promoter (i.e., constitutive or inducible) [32].

We here generated novel yeast models that can conditionally express human TDP-43 (either WT or bearing ALS-related mutations), from either single or multiple copies of the coding sequence stably integrated in the yeast genome. Such yeast cell models displaying a finely tuned expression levels of TDP-43 were then used to investigate possible modulators of TDP-43 cytotoxicity.

Different large-scale approaches in yeast and other cell paradigms (*Drosophila* and human cells) supported the linkage between ALS/FTD and the function of intra- and extra-nuclear membrane-less organelles, identifying some nucleolar proteins, cytosolic stress granules components and nucleocytoplasmic trafficking factors as genetic modifiers (i.e., suppressors or enhancers) of the cytotoxicity triggered by ALS-related proteins, such as C9orf72 DPRs [33, 34]. Moreover, some nucleolar proteins have been identified as TDP-43 interactors in systematic MS-based approach in mammalian cells [35].

Among these proteins, we focused on the phosphoprotein nucleolin (NCL) in light of multiple aspects, including the following structural and functional features of the protein: (i) similarly to TDP-43, NCL is able to bind DNA/RNA molecules thanks to multiple RRM domains; (ii) NCL carries an intrinsically disordered C-terminal region able to interact with different functional partners; (iii) NCL is one of the most abundant non-ribosomal proteins in the nucleolus, where it plays fundamental roles in nucleolar assembly and function, rRNA and ribosome metabolism [36], which are critically perturbed in ALS and FTD [37]. Noteworthy, although mainly localized in the nucleolus, NCL is able to shuttle in the cytosol (and to the plasma membrane) where it contributes to the transport of RNA molecules and ribosomal proteins, playing roles in both nucleocytoplasmic trafficking, and several signaling pathways, such as cell proliferation and survival [38–40].

We are here providing evidence that NCL is able to act as a potent suppressor of TDP-43 toxicity, relieving the lethal damage induced by WT or ALS-mutant TDP-43 overexpression in yeast cells. Additional experiments in mammalian HEK293T cell models further support that the NCL overexpression can prevent TDP-43-dependent toxicity, reducing the formation of insoluble aggregates and restoring cell viability, possibly by the maintenance of the proper localization of TDP-43 in the nuclear compartment.

Methods

Yeast strains and plasmids.

All yeast strains and plasmids used in this study are listed in Supplemental Tables 1 and 2, respectively. Methods to generate yeast strains and plasmids are reported in the Supplemental methods section. Primers used are listed in Supplemental Table 3–6.

Yeast media, transformation and yeast cell viability assays.

Procedures for yeast growth and manipulation were performed according to standard protocols [41, 42].

Yeast cells were grown in standard rich media (10 g/L Bacto-yeast extract, 20 g/L Bacto-peptone) supplemented with 20 g/L of glucose or galactose as carbon source or in synthetic minimal media (1.7 g/L yeast nitrogen base without amino acids, 5 g/L ammonium sulfate) containing 20 g/L of glucose, raffinose or galactose and lacking the specific nutrients allowing for selection of transformed yeast clones. Media components were from Difco (Thermo Fischer Scientific), and auxotrophic requirements were from Sigma-Aldrich. Induction of gene expression under Gal1 promoter control was obtained by growing transformed yeast cells in raffinose containing medium for 16 hours, followed by dilution of the cultures to an optical density at 600 nm light adsorption (OD_{600}) of 0.1 and growth in galactose containing medium. Cells were routinely incubated at 30 °C.

The PEG/lithium acetate method was used to transform yeast [43] and then cells were plated on selective solid media.

Yeast cell viability was performed by measuring the ability of yeast cultures to grow on solid (spotting assays) and liquid media (OD_{600} culture turbidity measurements) [44]. In particular, for spotting assays, yeast cells were grown overnight at 30 °C in liquid media (SD or YP) containing raffinose. Cultures were then normalized to OD_{600} = 1, serially diluted and spotted onto synthetic solid media containing glucose or galactose and the auxotrophic requirements as needed. Plates were maintained at 30 °C for 2–3 days. Conversely, OD_{600} measurements were performed in a Microplate Reader spectrophotometer (TECAN) at a 600 nm wavelength (bandwidth 9 nm) with 15 flashes and 200 µl of culture per well. Briefly, three yeast clones were grown overnight in a raffinose containing medium (non-inducing condition), diluted in triplicate to OD_{600} = 0.1 in a galactose containing medium (inducing condition), and grown for 24 h. OD_{600} was then recorded immediately after the transfer (t_0) or after 24 h of growth (t_{24h}), in the galactose medium, and the OD_{600} ratio (t_{24}/t_0) was calculated. Data were then normalized to the mean ratio of control cultures CEN.PX IMX672 (hereafter abbreviated as CENPK).

Microscopy analyses of S. cerevisiae **cells.**

For fluorescence microscopy observations, cells grown for 6 h in a galactose-containing liquid medium were used, while for cell shape analysis by brightfield microscopy cells were cultured on galactose containing solid substrate for 2 days. In both cases, before microscopy analysis, harvested cells were washed and resuspended in PBS, and then mounted on a coverslip with a thin agar slab as described previously [45]. Cells were imaged using an inverted microscope (CTR6000, Leica) equipped with a Xenon lamp, a suited fluorescence excitation/dichroic/emission filter setting (λ_{ex} = 488 nm for the excitation of GFP) and a computer-assisted charge-coupled device camera (Hamamatsu Orca flash 4.0), which allowed the acquisition of digital micrographs for either fluorescence or brightfield microscopy.

For morphometric measurements, the cell length-to-width ratio was calculated on digitalized images using the Fiji ImageJ software.

Whole protein extraction from S. cerevisiae **cells.**

The extraction of proteins from yeast cells for Western blot (WB) and mass spectrometry (MS) analyses was performed as described elsewhere [46] with some modifications. Briefly, yeast cells were harvested by centrifugation (6,000 x g, 10 min, 4 °C). Cells were then resuspended in 0.1 M NaOH and incubated at room temperature for 20 min. After pelleting, cells were finally lysed by vortexing (2 min) in a buffer containing 62.5 mM Tris-HCl (pH 6.8), 2.3% (w/v) SDS and 10% (w/v) glycerol (buffer O). Lysates were boiled (3 min) and, after centrifugation to remove cell debris, protein quantification was performed in the supernatant using a bicinchoninic acid (BCA) assay kit (Thermo Fisher Scientific), according to the manufacturer's instructions.

Yeast sample preparation for tandem mass tag-based quantitative proteomics.

For tandem mass tag (TMT)-based quantitative proteomic analysis, protein extracts (50 µg) from three biological replicates of parental CENPK and TDP 1C yeast strains were processed according to the filter-aided sample preparation method [47], using filters with 10,000 Da as molecular weight cut-off (Sartorius). Briefly, filters were washed four times with 8 M urea and 100 mM triethylammonium bicarbonate (TEAB) buffer (Sigma-Aldrich) and then treated in 100 mM TEAB containing 25 mM dithiothreitol (45 min, 55 °C) to reduce disulphide bonds, and then in the same buffer (100 mM TEAB) containing 55 mM iodoacetamide (45 min in the dark, RT) to block reduced cysteine residues. Finally, filters were washed twice using 100 mM TEAB and, afterwards, protein digestion was performed by adding 100 µL of sequencing grade modified trypsin (20 $\mu g/mL^{-1}$ in 100 mM TEAB, pH 8.0) to each filter (18 h, 37 °C). After digestion, filters were subjected to two subsequent centrifugation step (14,000 × g, 10 min) adding 50 µL of 100 mM TEAB for peptide recovery. Peptide mixtures were then labelled using 6-plex TMT reagents (Thermo Scientific), and subjected to fractionation and purification as previously described [48]. The three biological replicates of CENPK samples were labelled with the 126.1 Th, 127.1 Th and 128.1 Th TMT mass tags, respectively, while the three TDP 1C samples were labelled with the 129.1 Th, 130.1 Th and 131.1 Th TMT mass tags, respectively. After labelling, the six samples were mixed in equal total protein amounts and subjected to a desalting step by means of pre-activated and pre-equilibrated C_{18} BioPure spin columns (The Nest Group). To reduce sample complexity, TMT-labelled peptides were fractionated by strong cation exchange fractionation (SCX) before liquid chromatography (LC) and MS. Briefly, labelled samples were diluted with 4 volumes of 0.1% formic acid and then applied to the SCX macro spin columns (The Nest Group). After two washings, retained peptides were stepwise eluted in 5 fractions containing increasing concentrations of ammonium formate (i.e., 100, 200, 300, 400, 500 mM). Prior to sample injection into the high-performance liquid chromatography-high resolution tandem mass spectrometry (HPLC-HRMS/MS) workstation, each fraction was desalted by means of the C_{18} BioPure spin columns. The five labelled fractions of each peptide extract were finally dried using a stream of nitrogen (RT) and suspended in 100 µL of 0.1% formic acid for the subsequent MS analysis.

HPLC-HRMS/MS analysis.

Relative quantification of yeast proteins was achieved using a hybrid quadrupole-orbitrap Q-Exactive (Thermo Fisher Scientific) mass spectrometer, coupled to a UHPLC system Ultimate 3000 (Thermo Fisher

Scientific). Each SCX fraction was separated on a reverse-phase analytical column (Aeris peptide C_{18}, 150 mm × 2.1 mm, 2.6 µm, Phenomenex) kept at 30 °C.

Elution solvents for peptide separation were water (A) and acetonitrile (ACN) (B), both containing 0.1% (v/v) formic acid. The chromatographic separation was carried out at a flow rate of 200 µL · min^{-1} (35 min) using a gradient elution with the following composition (expressed as A:B ratio): 97.5:2.5 for 1 min; from 97.5:2.5 to 70:30 in 19 min (following a linear gradient), from 70:30 to 50:50 in 4 min; from 50:50 to 5:95 in 2 min and maintained for 4 min to wash the column; then back to 97.5:2.5 (to re-equilibrate the system) in 0.5 min and maintained for 4.5 min. The injection volume was 10 µL.

Ion source capillary temperature was 325 °C, the sheath gas flow rate 35 (arbitrary instrument units), auxiliary gas flow rate 10 (arbitrary instrument units), S-lens voltage 55 V, heater temperature 325 °C, and the spray was optimised at 3 kV. The instrument operated in data-dependent mode with a top-7 acquisition method (i.e., a full MS scan at 70,000 resolution on the orbitrap, followed by the MS/MS fragmentation of the seven most intense ions). Full scan spectra were acquired using an automatic gain control (AGC) target of 3×10^6 ions, an injection time (IT) of 250 ms, an isolation window of 2.0 Th, and a scan range from 300 to 2000 Th. Higher energy C-trap dissociation (HCD) was performed with a NCE of 30, AGC target of $2 \cdot 10^5$ ions, an IT of 120 ms, a dynamic exclusion of 30 s and a resolution of 17,500. Fragmentation spectra were used for peptide identification and quantification, setting a fixed starting mass of 100 Th. To increase the number of identified peptides, each SCX fraction was analysed twice. To this purpose, the m/z values of peptides positively identified in the first analysis (as described in details in the next section) were used to create a static exclusion list that was then applied to a second HPLC-HRMS/MS analysis (under the same chromatographic and instrumental conditions) for each sample fraction.

Untargeted MS data analysis.

Raw files derived from HPLC-HRMS/MS runs were analysed with a MudPIT protocol using the Proteome Discoverer 1.4 software (Thermo Fisher Scientific) interfaced to a SEQUEST HT search engine (Thermo Fisher Scientific). All MS/MS data were searched against the UniProt *S. cerevisiae* database (3AUP000002311). Enzyme specificity was set to trypsin, and a maximum of one missed cleavage was allowed. The precursor and product ion mass tolerances were set to 10 ppm and 0.2 Da, respectively. Oxidation of methionine was selected as variable modification, while 6-plex TMT at N-termini and at lysine residues, and carbamidomethylation of cysteines were set as fixed modification. Relative quantification was performed directly by the Proteome Discoverer software and only unique peptides were considered for quantification purposes. Based on the Percolator algorithm, proteins were considered as correctly identified if at least 2 unique peptides were quantified with an individual q-value < 0.05. Proteins were then grouped according to the principle of maximum parsimony. For quantification, the reporter mass tolerance was set to 20 ppm. The software detected the reporter ions (126.1, 127.1, 128.1, 129.1, 130.1, 131.1 Th), and performed the quantification of relative peptide abundance normalizing the intensity of each reporter ion to that of CENPK 1 sample (126.1 Th). Normalized intensity values of

proteins derived from Proteome Discoverer were exported in an Excel spreadsheet, and the matrix was arranged for further analysis. The final fold-change of a given protein was calculated as the mean value of the normalized ratios (TDP 1C/CENPK) of the three replicates. Finally, a two-tailed t-test was performed, and only proteins with a ratio > 1.33 or < 0.77, and a p-value < 0.05, were considered over-expressed or under-expressed, respectively.

Parallel reaction monitoring.

The targeted MS-based parallel reaction monitoring (PRM) analysis was carried out in WT CENPK, and TDP-43 1C and 2C strains expressing, or not, NCL. To this end, 50 µg of yeast lysates from nine different cultures for WT CENPK and for each of the 4 different TDP-43 clones (for a total 45 samples) were prepared and processed according to the filter-aided sample preparation (FASP) method as described above. After digestion, peptide mixtures were acidified (pH < 3) by adding formic acid and desalted using BioPure C_{18} spin columns (The Nest Group), following manufacturer's instructions. Briefly, samples were loaded in pre-activated C_{18} spin columns, that were washed twice with 200 µL of 0.5% formic acid (v/v), and then peptides were eluted using 75% ACN containing 0.1% formic acid (v/v). Peptide extracts were dried under a stream of nitrogen and, immediately before HPLC-HRMS/MS analyses, dissolved in a solution (100 µL) containing 5% (v/v) ACN and 0.1% (v/v) formic acid to obtain a final concentration of 0.5 $\mu g \cdot \mu L^{-1}$ of protein digest. Confirmatory analyses were performed using the same HPLC-HRMS/MS apparatus described above operating in the PRM mode. Peptides were separated using the same chromatographic gradient described above. The scheduled PRM method was developed by recording and selecting the most intense charge state of the considered peptides and 4 diagnostic precursor-to-product ion transitions in serial injections of a representative yeast digest sample. The same was done for glyceraldehyde 3-phosphate dehydrogenase (GAPDH), which was chosen as housekeeping protein. PRM acquisition parameters were as follows: HCD fragmentation with normalized collision energy (NCE) of 27, AGC target of 5×10^5 ions, an IT of 120 ms, an isolation window of 1.6 Th with an offset of 0.4 Th. Two proteotypic peptides were selected for each protein included in the PRM analysis. The selected precursor-to-product ion transitions, together with the retention time and the instrumental settings used in the acquisition method are reported in Supplemental Table 7.

To ensure that no instrumental drift occurred during PRM analysis, a pooled sample prepared by mixing together equal amounts of peptide digests was injected and analysed at the beginning and at the end of the analytical sequence. The Skyline software (version 3.5.0.9191) [49] was used to assess the relative abundance of each peptide by calculating the total peak area under the curve (AUC) of the chromatographic peaks deriving from four precursor-to-product ion transitions recorded for target peptides. Each AUC value in the different samples was normalized to the AUC of the corresponding peptide calculated in the pooled sample. Protein abundance was then calculated by averaging the normalized peptide values calculated for the two monitored peptides. Then protein abundance values were further normalized to the GAPDH abundance calculated for each sample to obtain relative protein abundance values to be compared between WT CENPK and the different TDP-43 yeast strains (with or without NCL).

HEK293T cell culture and transfection.

HEK293T cells were grown in Dulbecco's modified Eagle medium (DMEM) supplemented with 10% (v/v) foetal bovine serum (FBS), 2 mM L-glutamine, 100 U/ml penicillin, and 100 µg/ml streptomycin and maintained at 37 °C in a humidified incubator with 5% CO_2. HEK293T cells were seeded at 25% of confluence in multi-well culture plates 24 h before transfection. Cells were (co-)transfected using the Lipofectamine 3000 transfection kit (Invitrogen) following the manufacturer's instructions and analysed 48 h after transfection. Plasmids used to transfect HEK293T cells are reported in Supplemental Table 2. Details regarding the construction of plasmids are described in the Supplemental Methods section.

HEK293T cell viability assay.

Cell viability was assessed using the MTS [3-(4,5-dimethylthiazol-2-yl)-5-(3-carboxymethoxy-phenyl)-2-(4-sulfophenyl)-2H-tetrazolium, inner salt] assay (CellTiter96 Aqueous One 5 Solution Assay, Promega), based on the reduction of MTS by viable cells, following the manufacturer's instructions. Briefly, cells were seeded in 96-wells and co-transfected with the desired plasmids (as indicated in the figure legends), and – 48 h after transfection – the cell culture medium was removed and the MTS reagent [20 µl in 100 µl of phosphate-buffered saline (PBS)] was added to each culture well. Cells were then incubated at 37 °C (90 min), after which the absorbance of reduced MTS (λ = 490) was determined using a Microplate Reader (TECAN) spectrophotometer.

Confocal microscopy.

For confocal microscopy observations, HEK293T cells were seeded onto 13 mm coverslips and co-transfected using plasmids coding for the desired fluorescent constructs. 48 h after transfection, cells were rinsed twice with PBS, fixed (30 min, 4 °C) with paraformaldehyde [2% (w/v) in PBS], rinsed again and permeabilized (5 min, 4 °C) with Triton-X100 [0.1% (w/v) in PBS]. Cell nuclei were counter-stained with Hoechst 33342 [(5 µg/ml in PBS) 10 min, RT, Sigma-Aldrich], and coverslips were finally washed in PBS and mounted in Mowiol 40–88 (Sigma-Aldrich) [8% (w/v) in glycerol:PBS (1:3, v/v)]. Images were collected with a Leica SP5 confocal microscope using 40X or 63X HCX PL APO (NA 1.25 or 1.4, respectively) oil-immersion objectives. Laser excitation line, power intensity, and emission range were chosen accordingly to each fluorophore in different samples to minimize bleed-through. During acquisition, parameters for laser intensity and photomultiplier gain were kept constant. Imaging was performed at 1024 × 1024 pixels, with a 200 Hz acquisition rate, by capturing Z-series that covered the entire field of interest. Every planes of a Z-stack scan acquisition were merged into a single image using Fiji/ImageJ software.

HEK293T cell lysis and protein extraction.

For protein extraction, HEK293T cells, grown onto 12-wells plates and transfected as described above, were washed twice with ice-cold PBS and lysed with buffer O (60 µl/well). After centrifugation (14,000 · g,

10 min, 4 °C) to precipitate cell debris, the total protein content in the supernatant was determined by the BCA assay kit (Thermo Fisher Scientific).

Western blot and antibodies.

For Western blot (WB) analyses, 10–20 µg of proteins diluted in reducing sample buffer (buffer O added with 50 mM DTT and 0.01% (w/v) bromophenol blue) were subjected to SDS-PAGE [using 10% (w/v) acrylamide-N,N'-methylenebisacrylamide [37.5:1 (w/w)] or Mini-Protean TGX precast gels (4–15%, Bio-Rad Laboratories)] and electroblotted onto polyvinylidene difluoride (PVDF) membranes (0.45 µm pore size; Bio-Rad Laboratories). Membranes were stained with Coomassie brilliant blue (Sigma-Aldrich) to check for even protein loading, and digitalized images were collected for subsequent densitometric analysis. After Coomassie destaining with methanol, membranes were incubated (1 h, RT) in a blocking solution[5% (w/v) non-fat dry milk (Bio-Rad Laboratories) in TRIS-buffered saline (TBS) added with 0.1% (w/v) Tween-20 (TBS-T)], and then probed (overnight, 4 °C) with the desired primary antibody diluted in TBS-T containing 1% (w/v) bovine serum albumin (BSA). After three washings with TBS-T, membranes were incubated (1 h, RT) with horseradish peroxidase-conjugated anti-mouse or anti-rabbit IgG secondary antibody (Sigma-Aldrich, cat. no. A9044 and A0545, respectively) (1:60,000 in blocking solution), depending on the primary antibody. Immunoreactive bands were visualized using an enhance chemiluminescence reagent kit (EMD Millipore) and digitalized by means of an UVItec imaging system (Eppendorf). For densitometric analyses, the intensity of each immunoreactive band was normalized to the optical density of the corresponding Coomassie blue-stained lane [50].

The following primary antibodies (Abs) were used (dilutions in parentheses): anti-TDP-43 mouse monoclonal (m)Ab (1:1,000, Santa Cruz Biotechnology, cat. no. sc-376532); anti-NCL rabbit polyclonal (p) Ab (1:1,000; Santa Cruz Biotechnology, cat. no. sc-13057); anti GFP mouse mAb (1:2,000, Roche, cat. no.11814460001); anti RFP mouse mAb (1:5,000, Abcam, cat. no. 62341); anti BCL2 rabbit pAb (1:1,000, Sigma-Aldrich, cat. no. SAB4500003)); anti caspase 3 mouse mAb (1:1,000, Santa Cruz Biotechnology, cat. no. sc-56052); anti caspase 9 rabbit pAb (1:1,000, Sigma-Aldrich, cat. no. SAB4300683).

Protein co-immunoprecipitation from S. cerevisiae and HEK293T cell lysates.

For protein co-immunoprecipitation (co-IP) assays from *S. cerevisiae*, 10 ml of the TDP 2C yeast strain transformed with the NCL-mKATE2-pYES2 construct was grown for 8 h (reaching OD_{600} ~ 1) in galactose-rich medium, harvested by centrifugation (6,000 x g, 5 min) and resuspended in IP buffer [25 mM Tris-HCl (pH 7), 75 mM NaCl, 1 mM EDTA, 2.5% (w/v) glycerol, 0.2% (w/v) NP-40, 0.5 mM DTT, 1 mM PMSF and complete EDTA-free protease inhibitor cocktail (Roche)]. Cells were lysed by vortexing (30 s, 6000 rpm) in a MagnaLyser® apparatus (Roche Diagnostics). The protein fraction was obtained after precipitation of cell debris by centrifugation (14,000 x g, 10 min, 4 °C), and proteins were quantified by a Lowry assay kit (Sigma-Aldrich). 1 mg of total proteins (in IP buffer) was added with either 1 µg of anti-NCL rabbit pAb (Santa Cruz Biotechnology, cat. no. sc-13057), or anti-GFP mouse mAb (Roche, cat. no. 11814460001), or anti-RFP mouse mAb (Abcam, cat. no. 62341) antibody and incubated (16 h, 4 °C) under continuous

gentle inversion mixing. As negative control, the same amount of lysate was incubated in the absence of antibody.

The co-IP protocol for HEK293T cells was adapted from [35] with minor modifications. Briefly, cells co-transfected with the desired plasmids were resuspended in ice-cold lysis buffer (137 mM NaCl, 2.7 mM KCl, 8 mM Na_2HPO_4, and 2 mM KH_2PO_4, 0.2% NP-40, 10% glycerol (w/v), 5 mM EDTA and Roche complete EDTA-free protease inhibitor cocktail), and maintained on ice for 15 min. Cell lysates were then passed (5 times) through 21-gauge needles and centrifuged (20,000 × g, 4 °C, 15 min). The total protein content in the supernatant was determined using the BCA assay kit (ThermoFisher Scientific), and 200 µg of total proteins were incubated (16 h, 4 °C) with 0.2 µg of the rabbit polyclonal anti-NCL (Santa Cruz Biotechnology, cat. no. sc-13057) in lysis buffer under continuous gentle inversion mixing. When needed, cell lysates were treated with RNAse A (Thermo Fisher, cat. no. EN0531, 2 µg, 4 °C, 10 min) prior to immunoprecipitation. Non-transfected cells were processed as described above as negative control.

For both yeast and HEK293 samples, protein-antibody complexes were precipitated by adding protein A-Sepharose (2 mg, Sigma-Aldrich, cat. no. P3391). After incubation (1 h, 4 °C) under gentle shaking, sepharose bead-bound immunocomplexes were collected by centrifugation (3,000 × g, 4 °C), washed three times with lysis buffer and once with 50 mM Tris–HCl (pH 7.5), and finally boiled (3 min) in reducing sample buffer. Immunoprecipitated proteins were separated onto 10% SDS-PAGE gel, electroblotted onto PVDF membranes (Millipore) and analysed by WB with antibodies to target proteins.

Detergent-solubility assays in S. cerevisiae **and HEK293T protein extracts.**

The protocol for detergent-soluble and -insoluble protein fractionation from yeast cells was adapted from [51]. Briefly, 10 ml of yeast cultures grown for 6 h (reaching OD600 ~ 0.8-1) in inducing (galactose-rich) medium were harvested by centrifugation, washed with water and pelleted again. The cell pellet was resuspended in 500 µL of lysis buffer [25 mM Tris-HCl (pH 7.5), 75 mM NaCl, 1 mM EDTA, 2.5% glycerol (w/v), 0.5% Triton X-100 (v/v), 0.25% deoxycholate (w/v), 0.05% SDS (w/v), 0.5 mM DTT, 1 mM PMSF and complete EDTA-free protease inhibitor cocktail (Roche)]. Cells were lysed by vortexing (30 s · 6 times, 6,000 rpm) in a MagnaLyser apparatus (Roche Diagnostics), and a small fraction of the crude lysate (“total” fraction) was kept for subsequent analysis. The remaining crude lysate was centrifuged (800 · g, 5 min, 4 °C) to precipitate cell debris. Fractionation was performed by centrifuging (100,000 x g, 30 min, 4 °C) the cleared lysate, the supernatant (“detergent-soluble” fraction) was saved, and the pellet was resuspended in lysis buffer and centrifuged again as above. The final pellet (“detergent-insoluble” fraction) was resuspended in a urea-based buffer containing 7 M urea, 2 M thiourea, 4% CHAPS and 30 mM Tris (pH 8.5).

Detergent solubility fractionation of proteins from HEK293T cells was performed according to [52] with some modifications. Cells grown in 6-well plates and transfected as previously described were washed in PBS and harvested by centrifugation (2,000 · g, 5 min, 4 °C). Cells were then resuspended in 300 µL of radio-immunoprecipitation assay (RIPA) buffer [20 mM Tris-HCl (pH 7.5), 150 mM NaCl, 1% NP-40 (v/v),

0.1% sodium deoxycholate (w/v), 1 mM Na_3VO_4] supplemented with 2 mM EDTA, 1 mM EGTA and complete EDTA-free protease inhibitor cocktail (Roche). Following incubation on ice (15 min), cells were sonicated (10 s) and the obtained lysate was cleared by centrifugation (500 · g, 10 min) to remove cell debris. A small amount of the lysate ("total" fraction) was kept for subsequent analysis, while the remaining lysate was centrifuged (100,000 · g, 30 min, 4 °C). The resulting supernatant ("detergent-soluble" fraction) was saved and the pellet, after washing in RIPA buffer, was centrifuged again as above. The final pellet ("detergent-insoluble" fraction) was resuspended in the same urea-based buffer used for yeast samples.

The quantification of the protein content in all fractions of both yeast and HEK293T samples was carried out by the Lowry assay kit (Sigma-Aldrich). Protein fractions were then analysed by SDS/PAGE (using 10% (w/v) acrylamide-N,N'-methylenebisacrylamide [37.5:1 (w/w)) and WB for the detection of the target proteins as described previously.

Computational biology.

The protein–protein interaction network and gene ontology enrichment analysis was performed using the publicly available Cytoscape 3.7 software [53] integrated with the STRING application [54]. The STRING database uses a combination of prediction approaches integrated with other information (i.e., neighbourhood, transferred neighbourhood, gene fusion, co-occurrence, co-expression, experimental data, databases, text mining). The protein network was built using default parameters (minimum required interaction score = 0.4), including all active prediction parameters.

Statistical analysis.

Data were analysed using Prism 7 (GraphPad Software) and Microsoft Excel 2013 (Microsoft Corporation) software. Data are reported as mean ± standard error of the mean (SEM), with the number of experimental replicates (n) being indicated in the figure legends. Statistics was based on unpaired two-tailed Student's t-test, or by Kruskal-Wallis test followed by a Dunn's post hoc test, depending on the experiment, as indicated in the figure legends. A p-value < 0.05 was considered statistically significant (* $p < 0.05$, ** $p < 0.01$, *** $p < 0.001$, **** $p < 0.0001$).

Results

1) Generation and characterization of novel yeast models for TDP-43 proteinopathies.

As previously suggested by several reports, the toxic effects of human TDP-43 in yeast cells were directly correlated to the protein expression levels [30, 55, 56]. In the yeast models for TDP-43 proteinopathies that have been generated until now in *S. cerevisiae* strains with different genetic backgrounds (BY4741, W303), TDP-43 expression was driven by either constitutive or conditional (e.g., galactose-inducible) promoters, using integrative (single-copy) or non-integrative ectopic (low- or high-copy) plasmidic vectors in order to challenge yeast cells with low or high TDP-43 protein levels, respectively (reviewed in [30].

Since one chromosomally-integrated copy of TDP-43 displayed no (or little) toxicity to yeast cells [55], we generated (by CRISPR/Cas9 genome editing) novel *S. cerevisiae* yeast strains in the CEN.PK IMX672 genetic background [57] (hereafter abbreviated as CENPK), carrying in the yeast genome two (2C) or three (3C) integrated copies of the wild-type (WT) human TDP-43 sequence fused to GFP. To note that, as already demonstrated, the GFP-tagging did not affect the TDP-43-related toxicity in yeast [55]. The main purpose of this strategy was the generation of yeast models for TDP-43 proteinopathies that were better suited for the functional analysis of potential modulators of TDP-43 cytotoxicity compared to the previously established yeast paradigms, prevalently based on non-integrative multicopy (MC) plasmids. In order to prevent cell toxicity during normal cell growth, we placed the TDP-43-GFP transgene under the control of the tightly regulated galactose-inducible *GAL1* promoter, and inserted it into the yeast genome by replacing auxotrophic non-functional alleles (Supplemental Table 1). As controls, we also generated CENPK yeast strains carrying one copy (1C) of the TDP-43-GFP chimera integrated into the genome (by replacing a single auxotrophic non-functional allele), or strongly overexpressing the protein by means of an ectopic galactose-inducible 2 μ MC plasmid [55]. The genome editing correctness in the obtained yeast strains was verified by PCR (Supplemental Fig. S1). The expression of TDP-43 in the different yeast models at different time points after galactose induction was assessed by Western blot (WB) analysis, which confirmed that the protein expression levels were time- and dose/copy-dependent (Supplemental Fig. S2).

Firstly, we performed functional assays aimed at investigating the effects of TDP-43 expression on yeast viability. As shown in the spot test reported in Fig. 1A, the survival of yeast cells was unaffected in glucose-containing medium (TDP-43 expression off), whereas cells carrying two (or more) copies, but not one copy, of TDP-43 died when grown in galactose-containing medium (TDP-43 expression on). We further monitored the growth rate in liquid cultures of yeast strains carrying a different copy number of the TDP-43 construct (1C, 2C, 3C and MC) after 24 h of galactose induction compared to the CENPK control strain. As shown in Fig. 1B, while a single TDP-43 copy did not significantly affect yeast growth, the detrimental effects of TDP-43 on the growth rate increased with increasing the transgene copy number. Collectively taken, the above data indicate that TDP-43 cytotoxicity in the genetically engineered yeast strains correlated with TDP-43 copy number, thus to the extent of TDP-43 expression during the first hours after galactose induction (Supplemental Fig. S2).

Taking advantage from the GFP tag in the chimeric TDP-43 construct, we also visualized its intracellular distribution in yeast cells by fluorescence microscopy. As shown in Fig. 2A, TDP-43 fusion protein localized in discrete foci in all TDP-43-expressing yeast strains soon after induction (6 h). Our observation is consistent with previous findings reporting that yeast cells expressing TDP-43 (by one or more alleles) may contain a variable number of inclusion foci, which are also different in size and widely dispersed within the cells [58, 59].

We then addressed more precisely the issue of TDP-43 aggregation by biochemical separation of detergent-soluble and -insoluble fractions from total protein extracts, as previously described [19, 51]. Resulting data (Fig. 2B) showed that, after 6 h of induction, the majority of TDP-43 (~60%) was detected

in the insoluble fraction of all yeast strains carrying two or more copies of the transgene, contrary to what observed in the single-copy strain (in which only the ~40% of TDP-43 was found in the insoluble fraction), thereby correlating the formation of detergent-insoluble TDP-43 aggregates to the toxic effects of the protein.

It has been recently reported that the overexpression of human TDP-43 also affects cellular morphology in different yeast strains (i.e., BY4741 and W303), although the molecular mechanisms underlying such a defect remained unsolved [58]. We thus analyzed by optical microscopy the cell shape of yeast cells expressing TDP-43 from one or two integrated copies (after 48 h of induction in galactose), confirming that, in both cases, the expression of TDP-43 markedly perturbed cell morphology also in the CENPK genetic background, as already evident by visual inspection (Fig. 3A). A quantification of cell ellipticity (roughly measured as the ratio between the long and the short cell axis) substantiated a significant shape defect of the TDP-43-expressing yeast strains (Fig. 3B).

Notably, such a morphologic phenotype was specifically determined by the presence of TDP-43, but not by other ALS-related proteins. Indeed, although FUS/TLS or the C9orf72-derived PR dipeptide repeats (DPRs, PR50) caused the formation of numerous cytoplasmic inclusion foci and cell death in yeast [33, 60–64], they did not produce the elongated phenotype observed in TDP-43-expressing cells (data not shown).

A strict correlation between the elongated phenotype and cell death, however, is ruled out by the observation that such morphological defect also appears in yeast cells expressing non-toxic levels of TDP-43 (i.e., TDP 1C, Fig. 3).

In addition to WT TDP-43, we also generated yeast strains carrying either one or two chromosomal copies of (GFP-tagged) human TDP-43 bearing the ALS-related Q331K and M337V missense mutations that are known to exacerbate TDP-43 cytotoxicity [19]. These mutants resulted in effects that were comparable to those produced by the same amount of the WT protein. Indeed, a single allelic copy of the transgene did not affect yeast viability but induced the elongated morphologic phenotype (Supplemental Fig. S3), while two copies of both the TDP-43 mutant transgenes exerted detrimental effects on cell viability (Fig. 4A), growth rate (Fig. 4B) and cell morphology (Fig. 4C).

The above data demonstrated that expression of WT or ALS-associated mutant human TDP-43 markedly affects cell viability and growth in yeast strains carrying two or more copies of the transgene, while the expression of TDP-43 (either WT or mutated) from a single genomic copy was not sufficient to cause cell death. This finding supports the contention that TDP-43 cytotoxicity in yeast is dose-dependent [30, 55, 59] and is suggestive of a saturating toxic effect of two copies of the TDP-43 transgene, either WT or mutated, that correlates with the accumulation of detergent-insoluble aggregates of the protein.

This experimental evidence validates the use of the here presented yeast strains as valuable cell models for the identification of biological factors and/or chemical compounds that can rescue TDP-43-dependent harm.

2) TDP-43 cytotoxicity is suppressed by nucleolin (NCL).

Once established reliable yeast models for TDP-43 proteinopathies, we used such models to test the possible effects of NCL, which – as detailed in the Introduction - could be a promising player in the mechanisms of TDP-43 cytotoxicity. To this purpose, we overexpressed NCL (as a fusion construct with the red fluorescent protein mKate2) in the yeast strains bearing two or three integrated chromosomal copies of the TDP-43-GFP construct (WT or mutated), by means of an ectopic MC plasmid driven by a galactose-inducible promoter.

Both cell viability (Fig. 5A) and growth rate (Fig. 5B) assays demonstrated that NCL overexpression was able to rescue the negative effects of WT TDP-43-GFP overexpression from two, three or more (MC plasmid) gene copies. While NCL by itself did not result in any appreciable effect on cell viability (Fig. 5A), the protein also prevented the lethality induced by two chromosomally integrated copies of the Q331K and M337V TDP-43 mutants (Fig. 5C). Since we previously demonstrated that TDP-43 cytotoxicity strictly depends on the protein expression levels, we firstly ruled out the possibility that the rescue of the severe TDP-43-induced phenotypes by NCL could be caused by the downregulation of TDP-43-GFP amounts by NCL-mKate2 co-expression (Supplemental Fig. S4).

Notably, we also observed that the genetic 1:1 stoichiometry of NCL with respect to TDP-43 was not sufficient to prevent TDP-43 cytotoxicity, as demonstrated by the loss of viability of cells carrying two integrated chromosomal copies of both TDP-43-GFP and NCL-mKate2 constructs, driven by the same galactose-inducible promoter (Supplemental Fig. S5).

In the attempt to shed light on the ways by which NCL prevented TDP-43 toxicity, we next investigated the effects of NCL overexpression on TDP-43 behaviour and the TDP-43-related morphologic phenotype in yeast strains carrying two copies of the TDP-43 constructs. By biochemical fractionation assays, we found that the co-expression of NCL significantly increased the detergent-soluble fraction of WT TDP-43 (Fig. 6A), although NCL did not substantially changed the cellular distribution pattern of TDP-43-GFP in multiple discrete foci observed by fluorescence microscopy (data not shown). We also observed that the overexpression of NCL substantially (albeit not fully) reverted the morphological alterations of yeast cells triggered by two chromosomal copies of either WT and mutant (Q331K and M337V) TDP-43, as indicated by the significant recovery of the normal cellular shape (Fig. 6B).

Notably, untagged NCL, expressed by a MC plasmid, still retained the capability to counteract TDP-43 toxicity, as demonstrated by a cell viability assay (Supplemental Fig. S6), ruling out any potential effect of the mKate2 tag.

Collectively taken, the above data indicated that NCL overexpression was able to potently counteract the toxic effects of TDP-43 in yeast cells, and that such beneficial effect could be related to the aggregation dynamics of TDP-43, i.e., NCL reduced the detergent-insoluble fraction of TDP-43.

Additional experiments demonstrated that the relationship between TDP-43 and NCL was highly specific. Indeed, NCL overexpression failed to rescue the cytotoxicity caused in yeast cells by the expression of other ALS-related proteins (i.e., FUS/TLS and C9orf72 PR50 DPRs) by multicopy plasmids (Supplemental Fig. S7, panels A and B, respectively). On the other hand, TDP-43 cytotoxicity (in the two-copy strain) was not alleviated by the overexpression of other human NCL-related nucleolar proteins, such as its functional partner nucleophosmin (NPM, [65]), or the yeast NCL putative orthologue Nsr1p [66] (Supplemental Fig. S7, panels C and D, respectively). Since Nsr1p had been previously found to weakly enhance the toxicity of C9orf72-DPRs in yeast [33], we also explored TDP-43 toxicity (and the effects of NCL co-expression) in a mutant yeast strain bearing multiple TDP-43-GFP gene copies and depleted of the *NSR1* gene. We found that *NSR1* deletion did not impinge on the toxic phenotype induced by TDP-43 overexpression and that the ability of NCL to suppress TDP-43 toxicity was unperturbed in the *ΔNSR1* genetic background (Supplemental Fig. S8).

3) Mechanisms of the NCL suppressive effect on TDP-43 toxicity.

We then applied different approaches aimed at exploring the mechanisms by which NCL was able to counteract the TDP-43-related toxic phenotypes.

3.1 Proteomic analysis of TDP-43- and TDP-43/NCL-expressing yeast cells.

We firstly performed, by mass spectrometry (MS), a tandem mass tag (TMT)-based proteomic profiling of the yeast strain carrying 1 copy (non-toxic) of TDP-43 (TDP 1C) compared to the unmodified control strain (i.e., CENPK), both grown to log phase in raffinose medium (non-inducing) and transferred to galactose medium for 24 h to induce transgene expression. By this assay, carried out on three different clones for each strain, a total of 631 proteins were properly identified and quantified in all biological replicates of both strains. Interestingly, only 38 proteins were either significantly (p-value < 0.05) up-regulated (TDP-43/CENPK ratio > 1.33, 28 proteins) or down-regulated (TDP-43/CENPK ratio < 0.77, 10 proteins) in the TDP-43 1C strain (Supplemental Table 8).

In order to clarify which cellular processes could be altered by TDP-43 expression, we searched for interaction networks among the above 38 deregulated proteins in the TDP-43 1C strain through a computational analysis using the STRING software (Fig. 7A). Such a functional enrichment analysis indicated that these deregulated proteins were strictly correlated (PPI enrichment p-value < 10^{-16}) and that the vast majority of them belonged to discrete clusters. Notably, a gene ontology (GO) analysis showed that the most enriched cluster of up-regulated proteins included proteins involved in cellular response to stress, such as heat and oxidative stress, and oxidant detoxification (Supplemental Table 9).

We chose the 21 most up/down-regulated proteins (TDP-43/CENPK ratio > 1.50 and < 0.66, respectively, Supplemental Table 8) for a subsequent targeted validation study by a MS-based parallel reaction monitoring (PRM) approach, in both TDP 1C and 2C strains compared with control cells. This analysis confirmed the deregulation found by the previous untargeted approach for 1 protein (MAL11) out of the chosen 21 in the 1C strain only, 3 proteins in the 2C strain only (MTCU1, HFA1, heat shock protein

(HSP)12) and 16 proteins in both transgenic strains (Fig. 7B). Again, most of up-regulated proteins were those implicated in stress response by the previous GO analysis, while most of the down-regulated proteins were involved in proton transmembrane transport and in biosynthetic processes (Supplemental Table 9). Conversely, the PRM analysis did not confirm the deregulation for one protein (AIM17) in either transgenic strain (Fig. 7B).

The PRM approach was also used to assess the effects of NCL co-expression (by a MC plasmid) on the levels of the subset of 20 proteins that were mostly deregulated by TDP-43 expression (in both the 1C and 2C strains) according to the unbiased proteomic analysis, and whose alteration was confirmed by the validation study of Fig. 7B. We decided to exclude MAL11 and OYE3 from this analysis because MAL11 amounts were confirmed to be increased in the TDP 1C but not in the TDP 2C strain (Fig. 7B), while OYE3 is a yeast NADPH oxidoreductase with no *bona fide* orthologues in mammals. Remarkably, we found that NCL partially restored the effects of TDP-43 on the expression of 5 proteins out of the chosen 20 in the 1C strain, 5 proteins in the 2C strain and 1 protein (HSP82) in both transgenic strains (Figs. 7C and 7D) and that most of these proteins belonged to the stress response GO cluster (Supplemental Table 9).

In summary, the MS data indicated that the expression of TDP-43 (in the TDP 1C strain) triggered weak changes (~6%) of the whole yeast proteome, resulting, however, in the significant up-regulation of specific proteins implicated in the response to oxidative and heat stress and in protein folding and refolding processes that may be related to a proteostatic stress induced by TDP-43 expression. Most importantly, we also found that NCL brought the levels of some of these proteins in TDP-43-expressing strains towards the values observed in control cells, suggesting that it could act in some ways on the proteostatic stress associated to TDP-43 intoxication.

3.2 NCL cellular localization.

As mentioned, human NCL prevalently localizes in the nucleolar compartment where it plays multiple roles (e.g., ribosome biogenesis), but it may also translocate outside the nucleus taking part to nucleocytoplasmic trafficking [39, 67]. We therefore addressed the issue of whether the NCL-mediated suppression of TDP-43 noxious effects required the nuclear/nucleolar localization of the protein, by removing the nuclear localization sequence (NLS) of NCL (amino acids 279–298, Creancier et al., 1993). Viability assays demonstrated that the ΔNLS-NCL mutant still retains the ability to rescue TDP-43 toxicity (Fig. 8A). Conversely, the forced retention of NCL within the nucleus, by tagging the protein with the additional SV40 NLS sequence, resulted in the complete loss of NCL antagonizing effects against TDP-43 (Fig. 8B). Such a finding was further supported by the observation that chimeric proteins obtained by fusing NCL to nuclear-resident protein (i.e., the activation domain of GAL4 transcription factor) was completely unable to rescue TDP-43 cytotoxicity (Supplemental Figure S9).

These results strongly suggested the functional implication of the extranuclear fraction of NCL and the possible relevance of cytosolic processes involving the protein (e.g., nucleocytoplasmic trafficking, proteostatic stress and stress granule formation) in suppressing TDP-43 toxicity in yeast cells.

3.3 TDP-43/NCL physical interaction.

The above described genetic/functional interaction between TDP-43 and NCL might also be related to a physical interaction between the two proteins, considering that both proteins, although being mainly nuclear, may also localize in the cytosol [20, 67]. This possibility was suggested by a previous study showing – by immunoprecipitation of TDP-43 followed by identification of co-purified proteins by MS – that NCL was a physical interactor of TDP-43 in human epithelial kidney (HEK293T) cells [35]. We thus assayed if such a TDP-43-NCL physical association also occurred in yeast cells co-expressing TDP-43-GFP (in the strain bearing two chromosomally integrated copies of the transgene) and NCL-mKate2. By co-immunoprecipitation (co-IP) assays we found that a significant amount of the TDP-43-GFP chimera bound to NCL as demonstrated by its presence in the NCL-immunoprecipitated fraction (Supplemental Fig. S10A). Consistently, proteins co-immunoprecipitated by an anti-GFP antibody (pulling down the TDP-43-GFP chimera) contained NCL-mKate2, and – vice versa – TDP-43-GFP co-immunoprecipitated with NCL-mKate2 by an anti-mKate2 antibody, providing further support to the interaction of the two proteins in yeast (Supplemental Fig. S10B).

4) NCL antagonizes TDP-43 cytotoxicity and aggregation in human cells, promoting TDP-43 nuclear localization.

We next asked if NCL was able to suppress the TDP-43-induced phenotypes observed in the yeast models also in mammalian cells. To answer this question, we overexpressed human TDP-43 and NCL in the immortalized human cell line HEK293T by transient transfection with plasmids encoding fluorescence-tagged TDP-43-mKate2 and NCL-GFP chimeric constructs (see Supplemental Table 2 and Supplemental Methods).

We firstly assessed the viability of transfected cells by the MTS assay. Cells overexpressing the TDP-43 (either WT or bearing the Q331K missense mutation) chimera were significantly less viable (around 50%) compared to control cells (i.e., cells co-transfected with plasmids encoding GFP and mKate-2 only, Fig. 9A), highlighting the cytotoxic potential of TDP-43 overexpression in human cells, as already reported [69]. Co-expression of the NCL-GFP construct strikingly antagonized the deadly effects of both WT and mutant TDP-43 (Fig. 9A), indicating that NCL exerts a protective effect against TDP-43 toxicity also in mammalian cells.

In order to better clarify the mechanisms of TDP-43-induced toxicity, we analyzed the activation of the intrinsic apoptotic pathway that has been implicated in TDP-43 proteinopathies [70–73]. To this purpose, we examined by WB the amount of the anti-apoptotic protein Bcl-2, and of procaspase-3 and procaspase-9 whose cleaved products are executors of the apoptotic process [74]. We found that (both WT and Q331K) TDP-43 overexpression reduced the amounts of Bcl-2 and of full-length (inactive) caspases, demonstrating the activation of the intrinsic apoptotic pathway, which – importantly – was remarkably reversed by the co-expression of NCL (Fig. 9B).

Since TDP-43 delocalization to the cytoplasm, and its consequent depletion from the nucleus, is a prominent pathological feature in ALS and related TDP-43 proteinopathies [18, 20], we thus evaluated by confocal microscopy the cell distribution of overexpressed (WT or Q331K) TDP-43-mKate2 in HEK293T cells, in the absence or the presence of overexpressed NCL-GFP. As shown in Fig. 10 (panels A and B), NCL overexpression remarkably increased the fraction of cells in which TDP-43 was correctly localized to the nucleus, thereby reducing its (toxic) accumulation in the cytoplasm. In keeping with the idea that extra-nuclear delocalization of TDP-43 correlates with its accumulation in cytosolic aggregates, we found that the fraction of cells with (WT or mutant) TDP-43-mKate2 aggregation foci was significantly lower in the presence of NCL-GFP (Fig. 10, panels A and C). The quantification of the detergent-soluble and detergent-insoluble protein fractions of TDP-43-mKate2 in the absence or the presence of NCL-GFP by biochemical fractionation of HEK293T lysates was also consistent with this finding. Indeed, mirroring what observed in yeast cells, NCL was able to significantly reduce the insoluble TDP-43 fraction of both the WT and the Q331K mutant protein (Fig. 10D).

Taken together, the above data demonstrated that the overexpression of TDP-43 (either WT or bearing the ALS-associated Q331K missense mutation) was toxic to, and formed detergent-insoluble aggregates in, HEK293T cells and that NCL was able to attenuate both phenotypes, facilitating the nuclear localization of TDP-43. These data substantiated a functional role of NCL in antagonizing TDP-43 proteinopathies.

Finally, following the co-IP observations in yeast cells (Supplemental Fig. S10) and the previous finding that TDP-43 and NCL can interact in HEK293T cells [35], we checked if the physical association between the two proteins (i.e., TDP-43-mKate2 and NCL-GFP) also occurred in our experimental paradigm. Although we did never observe a clear colocalization of NCL and TDP-43 by fluorescence/confocal microscopy (e.g., see Fig. 10), possibly due to the strong nucleolar NCL signal, the co-IP experiments reported in Fig. 11 confirmed the interaction between the two proteins. This brought further support to the notion that the beneficial effects of NCL could be related to its physical association to TDP-43. Importantly, RNA – which may be bound by TDP-43 and NCL – does not seem to be involved in such an interaction, since treatment of cell lysates with RNase did not hamper the co-IP of the two proteins.

Discussion

Identifying modifiers of TDP-43 toxicity and understanding the cell pathways altered by TDP-43 mislocalization and aggregation could unveil novel therapeutic strategies for a set of NDs, collectively referred to as TDP43-related proteinopathies, including ALS, FTD and a proportion of AD cases.

TDP-43-mediated neurodegeneration is characterized by two major hallmarks: the depletion of nuclear TDP-43 and the concomitant accumulation of the protein in cytoplasmic aggregates, suggesting that TDP-43 proteinopathies are caused from either a loss of function, by impairing TDP-43 normal function in regulating transcription and mRNA processing, or a gain of function process, or both [13, 75].

Like other NDs caused protein misfolding and aggregation, also TDP-43 proteinopathies have been efficiently modelled in *S. cerevisiae* [31, 76, 77], mainly by the use of ectopic plasmids leading to TDP-43

overexpression and toxicity in yeast cells. However, the use of low- or high-copy plasmids displayed large variations of the effective number of the TDP-43 transgene in the yeast cells, failing to precisely relate cytotoxicity to protein expression levels, while the use of integrative vectors, stably introducing a single TDP-43 transgene copy in the yeast genome did not result in cell toxicity.

Taking advantage of the efficiency of the CRISPR/Cas9 system to perform genome editing in *S. cerevisiae*, we successfully integrated in specific genomic sites of yeast cells one, two or three copies of the full-length human TDP-43 cDNA (as a GFP-linked chimeric construct) under the control of the inducible GAL1 promoter. Thanks to this strategy we established a novel yeast model of TDP-43 proteinopathy that correlates TDP-43 toxicity with the number of transgene copies carried by yeast cells, thereby demonstrating that two genomic copies of the human TDP-43 transgene were necessary and sufficient to cause complete lethality in yeast cells (Fig. 1). Importantly, we correlated TDP-43-dependent cytotoxicity to the detergent solubility of the overexpressed protein, pinpointing the relevant role of TDP-43 aggregation for its toxic effects to yeast cells, since the majority of TDP-43 protein in the affected cells, carrying two or more transgene copies, partitioned into the detergent-insoluble fractions, differently from fully viable yeast cells carrying one TDP-43 transgene copy (Fig. 2).

We also analysed the effects of two ALS-linked TDP-43 missense mutations (i.e., Q331K and M337V), that were previously reported known to increase TDP-43 toxicity in yeast cells [19, 78]. However, according to a more recent study [59], we found that both disease-associated mutants behaved like the WT protein, as no cytotoxicity was observed when mutant proteins were expressed by a single genomic copy (Fig. S3). In addition, their effects to yeast viability in strains carrying two transgene copies were comparable to those of WT TDP-43, further supporting that TDP-43 cytotoxicity in yeast cells was dose-dependent [30, 55] and demonstrating a saturating effect of two copies of either WT or mutant TDP-43 transgene in the yeast genome.

Our models also recapitulated the alterations of yeast cell morphology caused by TDP-43 expression (Fig. 3) that were recently described [58], but the mechanisms and the significance of such a peculiar shape modification remain to be determined. Filamentous growth of yeast cells may be induced to preserve cell survival under stress conditions (e.g., nitrogen starvation), by the activation of several signalling pathways converging to the transcriptional activation of specific genes, primarily *FLO11* [79, 80]. In addition, yeast cell shape can also be perturbed by dysfunctions of key cellular processes, such as autophagy [79, 81] or nucleocytoplasmic trafficking [82], both of which have already been associated to TDP-43 function/toxicity [83, 84].

Whatever the mechanism, the presence of such morphologic phenotype also in yeast strains carrying a single copy of the TDP-43 transgene clearly indicated that, although very specific (i.e, FUS/TLS, nor C9orf72 DPRs resulted in such a morphologic alteration), it was completely unrelated to the lethal phenotype triggered by TDP-43 expression.

We sought to unveil the molecular mechanisms triggering the above described TDP-43-dependent phenotypes in yeast cells, by a large-scale proteomic analysis, which identified several proteins that were

dysregulated by TDP-43 expression, either at non-toxic or toxic levels. In particular, we found the expression of some chaperone proteins, belonging to the HSP subfamily involved in stress response, to be upregulated, possibly to counteract the protein misfolding stress induced by TDP-43, even at low expression levels. Conversely, no evident alterations were observed for proteins directly involved in nucleocytoplasmic trafficking, while our MS-based approach failed in detecting and/or quantifying proteins implicated in filamentous growth and autophagy regulation.

Taken together, the above findings demonstrated that the novel models here generated were able to recapitulate in a more stable genetic context the major effects of TDP-43 expression in yeast cells, i.e., cytotoxicity, protein aggregation dynamics, and specific morphological alterations, and were therefore suited for the identification of possible antagonists of TDP-43-induced cellular damage and to investigate the cell pathways thereof.

As mentioned, a prominent hallmark of ALS/FTD was the extra-nuclear translocation of TDP-43 and its accumulation in cytoplasmic insoluble inclusions in the central nervous system [14]. Consistently, several recent works strongly suggested that a common disease mechanism in ALS/FTD is the TDP-43-mediated impairment of nucleocytoplasmic trafficking [85, 86]. Notably, cytoplasmic TDP-43-inclusions in neurons are enriched in proteins that constitute the nuclear pore and take part in the nucleocytoplasmic transport machinery, thereby perturbing nuclear protein import and RNA export [84].

In light of the above notions, we focused our attention on NCL as a possible modifier of TDP-43 cytotoxicity. Indeed, NCL was reported as (one of) the most abundant nucleolar protein and is the first identified RNA binding protein able to shuttle from nucleus to cytoplasm, being involved in the transport of RNA molecules and proteins across the nuclear membrane [38, 39]. Importantly, NCL was also identified as a modifier of C9orf72-mediated cell toxicity in a *Drosophila* model [34], although no further investigation on this issue has been reported. Furthermore, NCL was included among the numerous TDP-43 interacting proteins involved in RNA metabolism which were identified through a global proteomic approach on HEK293T cells overexpressing TDP-43 [35].

Another link between NCL and ALS/FTD was suggested by the co-segregation of NCL and some RNA binding protein, including TDP-43, C9orf72 and FUS/TLS, in RNA foci accumulated in ALS patient tissues, resulting in the altered expression of specific RNA targets, RNA misprocessing events and disruption of nucleolar functions [87–92].

Moreover, NCL was also reported to play a role in the long-term maintenance of mature neurons [93], and has been related to other NDs because – in particular – its interaction with α-synuclein and DJ-1 that are critically involved in PD. Concurrently, NCL expression levels in the *substantia nigr*a of human PD patients were found to be dramatically reduced, suggesting an involvement of NCL depletion in the progression of PD and endorsing NCL as a possible target for therapeutic approaches [94].

In this work we provided evidence that NCL can potently counteract the detrimental effects of TDP-43 expression in both yeast and mammalian cells (Figs. 5,9). Our data indicated that NCL was able to

increase the solubility of TDP-43 (WT or bearing ALS-related missense mutations), and to suppress its cytotoxic effects (Figs. 6,10). Importantly, data from human HEK293T cells indicated that NCL overexpression markedly decreased the number of cells with cytoplasmic TDP-43 aggregates, while concurrently increasing the number of cells displaying proper TDP-43 nuclear localization (Fig. 10). We further observed that the TDP-43-dependent activation of apoptotic cell death in human cells was significantly reduced by NCL co-expression (Fig. 9), suggesting that NCL could suppress TDP-43 toxicity also by directly acting as an antiapoptotic factor, in light of its reported ability to stabilize the mRNA of the Bcl-2 anti-apoptotic factor [95–97], and to modulate p53 signalling at multiple levels [98–100]. We indeed observed that NCL overexpression was able to rescue the normal Bcl-2 levels in TDP-43 overexpressing HEK293T cells, without, however, affecting Bcl-2 expression in cells expressing endogenous TDP-43 amounts. Moreover, in yeast cells, NCL was not able to counteract the cytotoxicity induced by the overexpression of FUS and C9orf72 DPR, which were both recognized to induce cell death via the mitochondrial apoptotic pathway, similarly to TDP-43 [70, 101, 102]. Taken together, such data strongly suggest that NCL acts upstream of the apoptotic cascade triggered by TDP-43 overexpression, possibly by reducing the accumulation of cytosolic TDP-43 aggregates, thereby possibly preventing the activation of ER stress-related apoptotic cell death [73, 103, 104].

Further studies are needed to establish the exact mechanisms by which NCL specifically target TDP-43 pathology. However, the observation that the removal of the NLS did not influence NCL ability to rescue TDP-43 toxicity, which was conversely abrogated by introducing an additional NLS signal forcing NCL retention in the nuclear compartment (Fig. 8), strongly suggesting that the extranuclear localization of NCL, possibly linked to its nucleocytoplasmic shuttling role, is required to suppress TDP-43 proteotoxicity.

According to the evidence provided by this work a possible scenario could be proposed, whereby the extranuclear fraction of NCL interacts with TDP-43 in the cytosol, restoring its correct movement across the nuclear membrane and promoting its nuclear localization and solubility, therefore preventing the formation of cytosolic TDP-43 aggregates, and finally alleviating the proteostatic stress induced by TDP-43 overexpression and/or disease-related mutations. Concurrently, another sensible hypothesis entails that NCL exerts a chaperone-like activity for TDP-43, as already for histones, whereby NCL helps histone nuclear import and storage when not assembled with DNA [105, 106]. By this activity, NCL would promote TDP-43 proper folding and nuclear re-localization, thus preventing its cytosolic aggregation.

Conclusions

Although the above mechanistic propositions need further investigations, the here reported findings clearly identified NCL as a powerful modifier of TDP-43 proteotoxicity in both yeast and mammalian cells. NCL can then be considered as a means to understand the mechanisms of TDP-43-associated proteinopathies and a possible therapeutic target for ALS and related disorders.

Abbreviations

AD
Alzheimer’s disease
ACN
Acetonitrile
ALS
amyotrophic lateral sclerosis
AUC
area under the curve
DPRs
dipeptide repeats
FTD
frontotemporal dementia
FUS/TLS
fused in sarcoma/translocated in liposarcoma
HD
Hungtington’s disease
HPLC-HRMS/MS
high-performance liquid chromatography-high resolution tandem mass spectrometry
HSP
heat shock protein
MS
Mass spectrometry
NCE
normalized collision energy
NCL
nucleolin
NDs
neurodegenerative diseases
NLS
nuclear localization sequence
NPM
Nucleophosmin
PD
Parkinson’s disease
PRM
parallel reaction monitoring
RRM
RNA recognition motifs
SCX
strong cation exchange fractionation

TDP-43
Transactive Response DNA binding 43 kDa protein
TEAB
triethylammonium bicarbonate

Declarations

Ethical approval and consent to participate

Not applicable

Consent for publication

Not applicable

Availability of supporting data

All data used and analyzed for the current study are available from the corresponding author on reasonable request.

Competing interests

The authors declare no competing interests.

Funding

This work was supported by grants from University of Padova (BIRD202151/20) to A.B. and institutional fundings (DOR) to R.L.

Authors Contribution

Conceptualization, R.L., A.B., C.P.; Methodology R.L., R.S., C.P.; Formal analysis, C.P., R.S., R.B.; Investigation, C.P., R.B., R.S., M.L.M., J.A., A.M., Resources, F.T., G.S., M.L.M.; Writing – Original Draft, R.L., A.B., C.P.; Writing – Review & Editing, R.L., A.B., C.P., F.T., M.L.M., G.S., R.S. ; Supervision, R.L., A.B.; Funding Acquisition, R.L. and A.B.

All authors read and approved the final manuscript.

Acknowledgments

Authors are grateful to Dr. Nadia Minicuci (CNR Institute, Padova) for helpful suggestions in statistical analyses.

References

1. Arnold SE, Toledo JB, Appleby DH, Xie SX, Wang L-S, Baek Y, et al. Comparative survey of the topographical distribution of signature molecular lesions in major neurodegenerative diseases. J Comp Neurol [Internet]. 2013;521:4339–55. Available from: https://doi.org/10.1002/cne.23430
2. Bayer TA. Proteinopathies, a core concept for understanding and ultimately treating degenerative disorders? Eur Neuropsychopharmacol [Internet]. 2015;25:713–24. Available from: http://www.sciencedirect.com/science/article/pii/S0924977X13001107
3. Ugalde CL, Finkelstein DI, Lawson VA, Hill AF. Pathogenic mechanisms of prion protein, amyloid-β and α-synuclein misfolding: the prion concept and neurotoxicity of protein oligomers. J Neurochem [Internet]. 2016;139:162–80. Available from: https://doi.org/10.1111/jnc.13772
4. Nakashima-Yasuda H, Uryu K, Robinson J, Xie SX, Hurtig H, Duda JE, et al. Co-morbidity of TDP-43 proteinopathy in Lewy body related diseases. Acta Neuropathol. Germany; 2007;114:221–9.
5. Amador-Ortiz C, Lin W-L, Ahmed Z, Personett D, Davies P, Duara R, et al. TDP-43 immunoreactivity in hippocampal sclerosis and Alzheimer's disease. Ann Neurol. 2007;61:435–45.
6. Banks GT, Kuta A, Isaacs AM, Fisher EMC. TDP-43 is a culprit in human neurodegeneration, and not just an innocent bystander. Mamm Genome. 2008;19:299–305.
7. Hasegawa M, Arai T, Nonaka T, Kametani F, Yoshida M, Hashizume Y, et al. Phosphorylated TDP-43 in frontotemporal lobar degeneration and amyotrophic lateral sclerosis. Ann Neurol. 2008;64:60–70.
8. Geser F, Brandmeir NJ, Kwong LK, Martinez-Lage M, Elman L, McCluskey L, et al. Evidence of multisystem disorder in whole-brain map of pathological TDP-43 in amyotrophic lateral sclerosis. Arch Neurol. United States; 2008;65:636–41.
9. Forman MS, Trojanowski JQ, Lee VM-Y. TDP-43: a novel neurodegenerative proteinopathy. Curr Opin Neurobiol. 2007;17:548–55.
10. Arai T, Hasegawa M, Akiyama H, Ikeda K, Nonaka T, Mori H, et al. TDP-43 is a component of ubiquitin-positive tau-negative inclusions in frontotemporal lobar degeneration and amyotrophic lateral sclerosis. Biochem Biophys Res Commun [Internet]. 2006;351:602–11. Available from: http://www.sciencedirect.com/science/article/pii/S0006291X06023187
11. Buratti E, Baralle FE. The molecular links between TDP-43 dysfunction and neurodegeneration. Adv Genet. United States; 2009;66:1–34.
12. Ratti A, Buratti E. Physiological functions and pathobiology of TDP-43 and FUS/TLS proteins. J Neurochem. 2016;138:95–111.
13. Cascella R, Capitini C, Fani G, Dobson CM, Cecchi C, Chiti F. Quantification of the Relative Contributions of Loss-of-function and Gain-of-function Mechanisms in TAR DNA-binding Protein 43 (TDP-43) Proteinopathies. J Biol Chem. 2016;291:19437–48.
14. Neumann M, Sampathu DM, Kwong LK, Truax AC, Micsenyi MC, Chou TT, et al. Ubiquitinated TDP-43 in frontotemporal lobar degeneration and amyotrophic lateral sclerosis. Science. United States; 2006;314:130–3.
15. Igaz LM, Kwong LK, Chen-Plotkin A, Winton MJ, Unger TL, Xu Y, et al. Expression of TDP-43 C-terminal fragments in vitro recapitulates pathological features of TDP-43 proteinopathies. J Biol

Chem. 2009;284:8516–24.

16. Nonaka T, Kametani F, Arai T, Akiyama H, Hasegawa M. Truncation and pathogenic mutations facilitate the formation of intracellular aggregates of TDP-43. Hum Mol Genet [Internet]. 2009;18:3353–64. Available from: https://doi.org/10.1093/hmg/ddp275
17. Buratti E. Chapter One - Functional Significance of TDP-43 Mutations in Disease. In: Friedmann T, Dunlap JC, Goodwin SFBT-A in G, editors. Academic Press; 2015. p. 1–53. Available from: http://www.sciencedirect.com/science/article/pii/S0065266015000073
18. Hergesheimer RC, Chami AA, de Assis DR, Vourc'h P, Andres CR, Corcia P, et al. The debated toxic role of aggregated TDP-43 in amyotrophic lateral sclerosis: a resolution in sight? Brain. 2019;142:1176–94.
19. Johnson BS, Snead D, Lee JJ, McCaffery JM, Shorter J, Gitler AD. TDP-43 is intrinsically aggregation-prone, and amyotrophic lateral sclerosis-linked mutations accelerate aggregation and increase toxicity. J Biol Chem. 2009;284:20329–39.
20. Prasad A, Bharathi V, Sivalingam V, Girdhar A, Patel BK. Molecular Mechanisms of TDP-43 Misfolding and Pathology in Amyotrophic Lateral Sclerosis [Internet]. Front. Mol. Neurosci. . 2019. p. 25. Available from: https://www.frontiersin.org/article/10.3389/fnmol.2019.00025
21. Ou SH, Wu F, Harrich D, García-Martínez LF, Gaynor RB. Cloning and characterization of a novel cellular protein, TDP-43, that binds to human immunodeficiency virus type 1 TAR DNA sequence motifs. J Virol. 1995;69:3584–96.
22. Buratti E, Dörk T, Zuccato E, Pagani F, Romano M, Baralle FE. Nuclear factor TDP-43 and SR proteins promote in vitro and in vivo CFTR exon 9 skipping. EMBO J. 2001;20:1774–84.
23. Wolozin B. Regulated protein aggregation: stress granules and neurodegeneration. Mol Neurodegener. 2012;7:56.
24. Harrison AF, Shorter J. RNA-binding proteins with prion-like domains in health and disease. Biochem J [Internet]. 2017;474:1417–38. Available from: https://doi.org/10.1042/BCJ20160499
25. DeJesus-Hernandez M, Mackenzie IR, Boeve BF, Boxer AL, Baker M, Rutherford NJ, et al. Expanded GGGGCC hexanucleotide repeat in noncoding region of C9ORF72 causes chromosome 9p-linked FTD and ALS. Neuron. 2011;72:245–56.
26. Bosco DA, Lemay N, Ko HK, Zhou H, Burke C, Kwiatkowski TJJ, et al. Mutant FUS proteins that cause amyotrophic lateral sclerosis incorporate into stress granules. Hum Mol Genet. 2010;19:4160–75.
27. Li YR, King OD, Shorter J, Gitler AD. Stress granules as crucibles of ALS pathogenesis. J Cell Biol. 2013;201:361–72.
28. Zhang Y-J, Gendron TF, Ebbert MTW, O'Raw AD, Yue M, Jansen-West K, et al. Poly(GR) impairs protein translation and stress granule dynamics in C9orf72-associated frontotemporal dementia and amyotrophic lateral sclerosis. Nat Med. 2018;24:1136–42.
29. Ruetenik A, Barrientos A. Exploiting Post-mitotic Yeast Cultures to Model Neurodegeneration [Internet]. Front. Mol. Neurosci. . 2018. p. 400. Available from: https://www.frontiersin.org/article/10.3389/fnmol.2018.00400

30. Armakola M, Hart MP, Gitler AD. TDP-43 toxicity in yeast. Methods [Internet]. Elsevier Inc.; 2011;53:238–45. Available from: http://dx.doi.org/10.1016/j.ymeth.2010.11.006
31. Kryndushkin D, Shewmaker F. Modeling ALS and FTLD proteinopathies in yeast: An efficient approach for studying protein aggregation and toxicity. Prion. 2011;5:250–7.
32. Karim AS, Curran KA, Alper HS. Characterization of plasmid burden and copy number in Saccharomyces cerevisiae for optimization of metabolic engineering applications. FEMS Yeast Res [Internet]. 2013;13:107–16. Available from: https://doi.org/10.1111/1567-1364.12016
33. Jovičič A, Mertens J, Boeynaems S, Bogaert E, Chai N, Yamada SB, et al. Modifiers of C9orf72 dipeptide repeat toxicity connect nucleocytoplasmic transport defects to FTD/ALS. Nat Neurosci. 2015;18:1226–9.
34. Lee K-H, Zhang P, Kim HJ, Mitrea DM, Sarkar M, Freibaum BD, et al. C9orf72 Dipeptide Repeats Impair the Assembly, Dynamics, and Function of Membrane-Less Organelles. Cell [Internet]. 2016;167:774-788.e17. Available from: http://www.sciencedirect.com/science/article/pii/S0092867416313836
35. Freibaum BD, Chitta RK, High AA, Taylor JP. Global analysis of TDP-43 interacting proteins reveals strong association with RNA splicing and translation machinery. J Proteome Res [Internet]. 2010;9:1104–20. Available from: https://pubmed.ncbi.nlm.nih.gov/20020773
36. Jia W, Yao Z, Zhao J, Guan Q, Gao L. New perspectives of physiological and pathological functions of nucleolin (NCL). Life Sci. Netherlands; 2017;186:1–10.
37. Ling S-C, Polymenidou M, Cleveland DW. Converging Mechanisms in ALS and FTD: Disrupted RNA and Protein Homeostasis. Neuron [Internet]. 2013;79:416–38. Available from: http://www.sciencedirect.com/science/article/pii/S0896627313006570
38. Borer RA, Lehner CF, Eppenberger HM, Nigg EA. Major nucleolar proteins shuttle between nucleus and cytoplasm. Cell. United States; 1989;56:379–90.
39. Tajrishi MM, Tuteja R, Tuteja N. Nucleolin. Commun Integr Biol [Internet]. Taylor & Francis; 2011;4:267–75. Available from: https://doi.org/10.4161/cib.4.3.14884
40. Wise JF, Berkova Z, Mathur R, Zhu H, Braun FK, Tao R-H, et al. Nucleolin inhibits Fas ligand binding and suppresses Fas-mediated apoptosis in vivo via a surface nucleolin-Fas complex. Blood [Internet]. 2013;121:4729–39. Available from: https://doi.org/10.1182/blood-2012-12-471094
41. Amberg DC, Burke D, Strathern JN, Burke D, Laboratory. CSH. Methods in yeast genetics : a Cold Spring Harbor Laboratory course manual. Cold Spring Harbor, N.Y.: Cold Spring Harbor Laboratory Press; 2005.
42. Vokes M, Carpenter A. Current Protocols in Molecular Biology. Curr Protoc Mol Biol. 2008;Chapter 14:Unit 14.17.
43. Gietz RD, Woods RA. Yeast transformation by the LiAc/SS Carrier DNA/PEG method. Methods Mol Biol. United States; 2006;313:107–20.
44. Mirisola MG, Braun RJ, Petranovic D. Approaches to study yeast cell aging and death. FEMS Yeast Res [Internet]. 2014;14:109–18. Available from: https://doi.org/10.1111/1567-1364.12112

45. Skinner S, Sepúlveda L, Xu H, Golding I. Corrigendum: Measuring mRNA copy number in individual Escherichia coli cells using single-molecule fluorescent in situ hybridization. Nat Protoc. 2013;8:1100–13.
46. Kushnirov V V. Rapid and reliable protein extraction from yeast. Yeast [Internet]. 2000;16:857–60. Available from: https://doi.org/10.1002/1097-0061(20000630)16:9%3C857::AID-YEA561%3E3.0.CO
47. Wisniewski JR, Zougman A, Nagaraj N, Mann M. Universal sample preparation method for proteome analysis. Nat Methods. United States; 2009;6:359–62.
48. Biancotto G, Bovo D, Mastrorilli E, Manuali E, Angeletti R, Stella R. TMT-Based Proteomics Profiling of Bovine Liver Underscores Protein Markers of Anabolic Treatments. Proteomics [Internet]. 2019;19:1800422. Available from: https://doi.org/10.1002/pmic.201800422
49. MacLean B, Tomazela DM, Shulman N, Chambers M, Finney GL, Frewen B, et al. Skyline: an open source document editor for creating and analyzing targeted proteomics experiments. Bioinformatics. England; 2010;26:966–8.
50. Colella AD, Chegenii N, Tea MN, Gibbins IL, Williams KA, Chataway TK. Comparison of Stain-Free gels with traditional immunoblot loading control methodology. Anal Biochem [Internet]. 2012;430:108–10. Available from: http://www.sciencedirect.com/science/article/pii/S0003269712004228
51. Alberti S, Halfmann R, Lindquist S. Biochemical, cell biological, and genetic assays to analyze amyloid and prion aggregation in yeast. Methods Enzymol. United States; 2010;470:709–34.
52. Cohen TJ, Hwang AW, Unger T, Trojanowski JQ, Lee VMY. Redox signalling directly regulates TDP-43 via cysteine oxidation and disulphide cross-linking. EMBO J [Internet]. Nature Publishing Group; 2012;31:1241–52. Available from: http://dx.doi.org/10.1038/emboj.2011.471
53. Shannon P, Markiel A, Ozier O, Baliga NS, Wang JT, Ramage D, et al. Cytoscape: a software environment for integrated models of biomolecular interaction networks. Genome Res. United States; 2003;13:2498–504.
54. Doncheva NT, Morris JH, Gorodkin J, Jensen LJ. Cytoscape StringApp: Network Analysis and Visualization of Proteomics Data. J Proteome Res. 2019;18:623–32.
55. Johnson BS, McCaffery JM, Lindquist S, Gitler AD. A yeast TDP-43 proteinopathy model: Exploring the molecular determinants of TDP-43 aggregation and cellular toxicity. Proc Natl Acad Sci U S A. 2008;105:6439–44.
56. Figley MD, Gitler AD. Yeast genetic screen reveals novel therapeutic strategy for ALS. Rare Dis. 2013;1:e24420.
57. Mans R, van Rossum HM, Wijsman M, Backx A, Kuijpers NGA, van den Broek M, et al. CRISPR/Cas9: A molecular Swiss army knife for simultaneous introduction of multiple genetic modifications in Saccharomyces cerevisiae. FEMS Yeast Res. 2015;15:1–15.
58. Park S-K, Hong JY, Arslan F, Kanneganti V, Patel B, Tietsort A, et al. Overexpression of the essential Sis1 chaperone reduces TDP-43 effects on toxicity and proteolysis. PLoS Genet. United States; 2017;13:e1006805.

59. Bolognesi B, Faure AJ, Seuma M, Schmiedel JM, Tartaglia GG, Lehner B. The mutational landscape of a prion-like domain. Nat Commun [Internet]. Springer US; 2019;10. Available from: http://dx.doi.org/10.1038/s41467-019-12101-z
60. Sun Z, Diaz Z, Fang X, Hart MP, Chesi A, Shorter J, et al. Molecular determinants and genetic modifiers of aggregation and toxicity for the als disease protein fus/tls. PLoS Biol. 2011;9.
61. Lindström M, Liu B. Yeast as a Model to Unravel Mechanisms Behind FUS Toxicity in Amyotrophic Lateral Sclerosis. Front Mol Neurosci. 2018;11:1–10.
62. Fushimi K, Long C, Jayaram N, Chen X, Li L, Wu JY. Expression of human FUS/TLS in yeast leads to protein aggregation and cytotoxicity, recapitulating key features of FUS proteinopathy. Protein Cell. 2011;2:141–9.
63. Ju S, Tardiff DF, Han H, Divya K, Zhong Q, Maquat LE, et al. A Yeast Model of FUS/TLS-Dependent Cytotoxicity. PLoS Biol. 2011;9.
64. Chai N, Gitler AD. Yeast screen for modifiers of C9orf72 poly(glycine-arginine) dipeptide repeat toxicity. FEMS Yeast Res. 2018;18:1–8.
65. Scott DD, Oeffinger M. Nucleolin and nucleophosmin: nucleolar proteins with multiple functions in DNA repair. Biochem Cell Biol [Internet]. NRC Research Press; 2016;94:419–32. Available from: https://doi.org/10.1139/bcb-2016-0068
66. Lee WC, Xue Z, Mélèse T. The NSR1 gene encodes a protein that specifically binds nuclear localization sequences and has two RNA recognition motifs. J Cell Biol. 1991;113:1–12.
67. Mongelard F, Bouvet P. Nucleolin: a multiFACeTed protein. Trends Cell Biol. 2007;17:80–6.
68. Creancier L, Prats H, Zanibellato C, Amalric F, Bugler B. Determination of the functional domains involved in nucleolar targeting of nucleolin. Mol Biol Cell. 1993;4:1239–50.
69. Lanznaster D, Bourgeais J, Bruno C, Hergesheimer RC, Thepault R-A, Vourc'h P, et al. TDP-43-Mediated Toxicity in HEK293T Cells: A Fast and Reproducible Protocol To Be Employed in the Search of New Therapeutic Options against Amyotrophic Lateral Sclerosis. Cells. 2019;9:68.
70. Suzuki H, Lee K, Matsuoka M. TDP-43-induced death is associated with altered regulation of BIM and Bcl-xL and attenuated by caspase-mediated TDP-43 cleavage. J Biol Chem. 2011;286:13171–83.
71. Vogt MA, Ehsaei Z, Knuckles P, Higginbottom A, Helmbrecht MS, Kunath T, et al. TDP-43 induces p53-mediated cell death of cortical progenitors and immature neurons. Sci Rep. 2018;8:1–13.
72. Mutihac R, Alegre-Abarrategui J, Gordon D, Farrimond L, Yamasaki-Mann M, Talbot K, et al. TARDBP pathogenic mutations increase cytoplasmic translocation of TDP-43 and cause reduction of endoplasmic reticulum Ca2+ signaling in motor neurons. Neurobiol Dis [Internet]. Elsevier B.V.; 2015;75:64–77. Available from: http://dx.doi.org/10.1016/j.nbd.2014.12.010
73. Wang X, Zhou S, Ding X, Ma M, Zhang J, Zhou Y, et al. Activation of ER stress and autophagy induced by TDP-43 A315T as pathogenic mechanism and the corresponding histological changes in skin as potential biomarker for ALS with the mutation. Int J Biol Sci. 2015;11:1140–9.

74. Ola MS, Nawaz M, Ahsan H. Role of Bcl-2 family proteins and caspases in the regulation of apoptosis. Mol Cell Biochem. Netherlands; 2011;351:41–58.
75. Lee EB, Lee VMY, Trojanowski JQ. Gains or losses: Molecular mechanisms of TDP43-mediated neurodegeneration. Nat Rev Neurosci [Internet]. Nature Publishing Group; 2012;13:38–50. Available from: http://dx.doi.org/10.1038/nrn3121
76. Sarto-Jackson I, Tomaska L. How to bake a brain: yeast as a model neuron. Curr Genet. 2016;62.
77. Braun RJ, Büttner S, Ring J, Kroemer G, Madeo F. Nervous yeast: modeling neurotoxic cell death. Trends Biochem Sci [Internet]. 2010;35:135–44. Available from: http://www.sciencedirect.com/science/article/pii/S0968000409001972
78. Lim L, Wei Y, Lu Y, Song J. ALS-Causing Mutations Significantly Perturb the Self-Assembly and Interaction with Nucleic Acid of the Intrinsically Disordered Prion-Like Domain of TDP-43. PLOS Biol [Internet]. Public Library of Science; 2016;14:e1002338. Available from: https://doi.org/10.1371/journal.pbio.1002338
79. Song Q, Kumar A. An Overview of Autophagy and Yeast Pseudohyphal Growth: Integration of Signaling Pathways during Nitrogen Stress. Cells. 2012;1:263–83.
80. Cullen PJ, Sprague GFJ. The regulation of filamentous growth in yeast. Genetics. 2012;190:23–49.
81. Ma J, Jin R, Jia X, Dobry CJ, Wang L, Reggiori F, et al. An interrelationship between autophagy and filamentous growth in budding yeast. Genetics. 2007;177:205–14.
82. Künzler M, Trueheart J, Sette C, Hurt E, Thorner J. Mutations in the YRB1 gene encoding yeast ran-binding-protein-1 that impair nucleocytoplasmic transport and suppress yeast mating defects. Genetics. 2001;157:1089–105.
83. Budini M, Buratti E, Morselli E, Criollo A. Autophagy and Its Impact on Neurodegenerative Diseases: New Roles for TDP-43 and C9orf72. Front Mol Neurosci. 2017;10:170.
84. Chou C-C, Zhang Y, Umoh ME, Vaughan SW, Lorenzini I, Liu F, et al. TDP-43 pathology disrupts nuclear pore complexes and nucleocytoplasmic transport in ALS/FTD. Nat Neurosci [Internet]. 2018;21:228–39. Available from: https://doi.org/10.1038/s41593-017-0047-3
85. Gasset-Rosa F, Lu S, Yu H, Chen C, Melamed Z, Guo L, et al. Cytoplasmic TDP-43 De-mixing Independent of Stress Granules Drives Inhibition of Nuclear Import, Loss of Nuclear TDP-43, and Cell Death. Neuron. 2019;102:339-357.e7.
86. Kim HJ, Taylor JP. Lost in Transportation: Nucleocytoplasmic Transport Defects in ALS and Other Neurodegenerative Diseases. Neuron. 2017;96:285–97.
87. Butti Z, Patten SA. RNA Dysregulation in Amyotrophic Lateral Sclerosis. Front Genet. 2018;9:712.
88. Haeusler AR, Donnelly CJ, Periz G, Simko EAJ, Shaw PG, Kim M-S, et al. C9orf72 nucleotide repeat structures initiate molecular cascades of disease. Nature. 2014;507:195–200.
89. Gitler AD, Tsuiji H. There has been an awakening: Emerging mechanisms of C9orf72 mutations in FTD/ALS. Brain Res. 2016;1647:19–29.

90. Simon-Sanchez J, Dopper E, Cohn-Hokke P, Hukema R, Nicolaou N, Seelaar H, et al. The clinical and pathological phenotype of C9ORF72 hexanucleotide repeat expansions. Brain. 2012;135:723–35.
91. Donnelly CJ, Zhang P-W, Pham JT, Haeusler AR, Mistry NA, Vidensky S, et al. RNA toxicity from the ALS/FTD C9ORF72 expansion is mitigated by antisense intervention. Neuron. 2013;80:415–28.
92. Zhou Y, Liu S, Oztürk A, Hicks GG. FUS-regulated RNA metabolism and DNA damage repair: Implications for amyotrophic lateral sclerosis and frontotemporal dementia pathogenesis. Rare Dis (Austin, Tex). 2014;2:e29515.
93. Hetman M, Pietrzak M. Emerging roles of the neuronal nucleolus. Trends Neurosci. 2012;35:305–14.
94. Caudle WM, Kitsou E, Li J, Bradner J, Zhang J. A role for a novel protein, nucleolin, in Parkinson's disease. Neurosci Lett. 2009;459:11–5.
95. Otake Y, Sengupta TK, Bandyopadhyay S, Spicer EK, Fernandes DJ. Retinoid-induced apoptosis in HL-60 cells is associated with nucleolin down-regulation and destabilization of Bcl-2 mRNA. Mol Pharmacol. United States; 2005;67:319–26.
96. Ishimaru D, Zuraw L, Ramalingam S, Sengupta TK, Bandyopadhyay S, Reuben A, et al. Mechanism of regulation of bcl-2 mRNA by nucleolin and A+U-rich element-binding factor 1 (AUF1). J Biol Chem. 2010;285:27182–91.
97. Cheng Y, Zhao G, Zhang S, Nigim F, Zhou G, Yu Z, et al. AS1411-Induced Growth Inhibition of Glioma Cells by Up-Regulation of p53 and Down-Regulation of Bcl-2 and Akt1 via Nucleolin. PLoS One. 2016;11:e0167094.
98. Saxena A, Rorie CJ, Dimitrova D, Daniely Y, Borowiec JA. Nucleolin inhibits Hdm2 by multiple pathways leading to p53 stabilization. Oncogene. England; 2006;25:7274–88.
99. Takagi M, Absalon MJ, McLure KG, Kastan MB. Regulation of p53 translation and induction after DNA damage by ribosomal protein L26 and nucleolin. Cell. United States; 2005;123:49–63.
100. Bhatt P, d'Avout C, Kane NS, Borowiec JA, Saxena A. Specific domains of nucleolin interact with Hdm2 and antagonize Hdm2-mediated p53 ubiquitination. FEBS J. 2012;279:370–83.
101. Braun R. Mitochondrion-mediated cell death: Dissecting yeast apoptosis for a better understanding of neurodegeneration. Front Oncol. 2012;2:182.
102. Dafinca R, Scaber J, Ababneh N, Lalic T, Weir G, Christian H, et al. C9orf72 Hexanucleotide Expansions Are Associated with Altered Endoplasmic Reticulum Calcium Homeostasis and Stress Granule Formation in Induced Pluripotent Stem Cell-Derived Neurons from Patients with Amyotrophic Lateral Sclerosis and Frontotemporal Deme. Stem Cells. 2016;34:2063–78.
103. Walker AK, Soo KY, Sundaramoorthy V, Parakh S, Ma Y, Farg MA, et al. ALS-associated TDP-43 induces endoplasmic reticulum stress, which drives cytoplasmic TDP-43 accumulation and stress granule formation. PLoS One. 2013;8:e81170.
104. Vaccaro A, Patten SA, Aggad D, Julien C, Maios C, Kabashi E, et al. Pharmacological reduction of ER stress protects against TDP-43 neuronal toxicity in vivo. Neurobiol Dis. United States; 2013;55:64–75.

105. Angelov D, Bondarenko VA, Almagro S, Menoni H, Mongélard F, Hans F, et al. Nucleolin is a histone chaperone with FACT-like activity and assists remodeling of nucleosomes. EMBO J [Internet]. 2006;25:1669–79. Available from: https://doi.org/10.1038/sj.emboj.7601046

106. Gaume X, Monier K, Argoul F, Mongelard F, Bouvet P. *In vivo* Study of the Histone Chaperone Activity of Nucleolin by FRAP. Corbett AH, editor. Biochem Res Int [Internet]. Hindawi Publishing Corporation; 2011;2011:187624. Available from: https://doi.org/10.1155/2011/187624

Figures

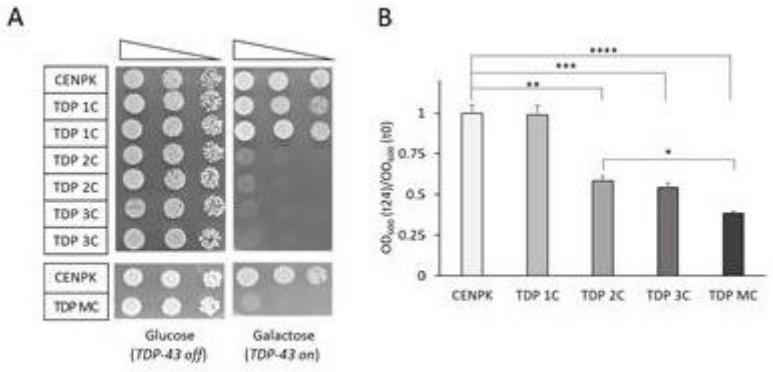

Figure 1

Two or more copies of the human TDP-43 transgene cause a lethal phenotype in S. cerevisiae. A. The spot test was used to assess the effect of increasing (galactose-inducible) expression of human TDP-43 on the viability of S. cerevisiae (strain CEN.PK IMX672, hereafter abbreviated as CENPK) in which one (TDP 1C), two (TDP 2C) or three (TDP 3C) copies of TDP-43 were integrated in the yeast genome, compared to the unmodified strain (CENPK) (upper panel). The effect of a non-integrative multi-copy plasmid coding for human TDP-43 (TDP MC) was also evaluated in the same S. cerevisiae strain compared to unmodified strain (CENPK) (lower panel). Three 10-fold serial dilutions for each strain (schematically indicated by the scales on the top), incubated onto glucose- or galactose-containing agar plates at 30 °C for 3 days, are shown. While in all cases yeast cells grown in a glucose-containing medium, in which TDP-43 expression is repressed (TDP-43 off), were fully viable, a toxic phenotype was readily appreciable when the expression of two or more copies of the TDP-43 transgene was induced by the presence of galactose in the culture medium (TDP-43 on). Conversely, the galactose-induced expression of TDP-43 from only one chromosomal copy of the transgene did not result in appreciable lethality. Data are representative of 3 experiments yielding comparable results. B. A quantitative measurement of the cell growth rate of the above yeast strains was performed by pre-culturing cells in a raffinose-containing medium overnight, and then by diluting cell cultures to OD600 = 0.1 in a medium containing galactose to induce the transgene expression. Cells were then cultured for further 24 h at 30 °C, when the cell growth rate was measured as the ratio of the OD600 at the end (t24) and the beginning

(t0) of culturing in the galactose medium (OD600 (t24)/OD600 (t0)). Data (mean ± standard error of the mean (SEM)) are reported after normalization to the mean value of the unmodified strain (CENPK). While TDP 1C cells do not differ from the parental CENPK control, yeast strains containing two or more transgene copies show a remarkably defective growth rate that decreases with increasing TDP-43 expression (see also Supplemental Fig. S2). n=12, *p<0.05, **p<0.01, ***p<0.001, ****p<0.0001 Kruskal-Wallis test followed by a Dunn's post hoc test.

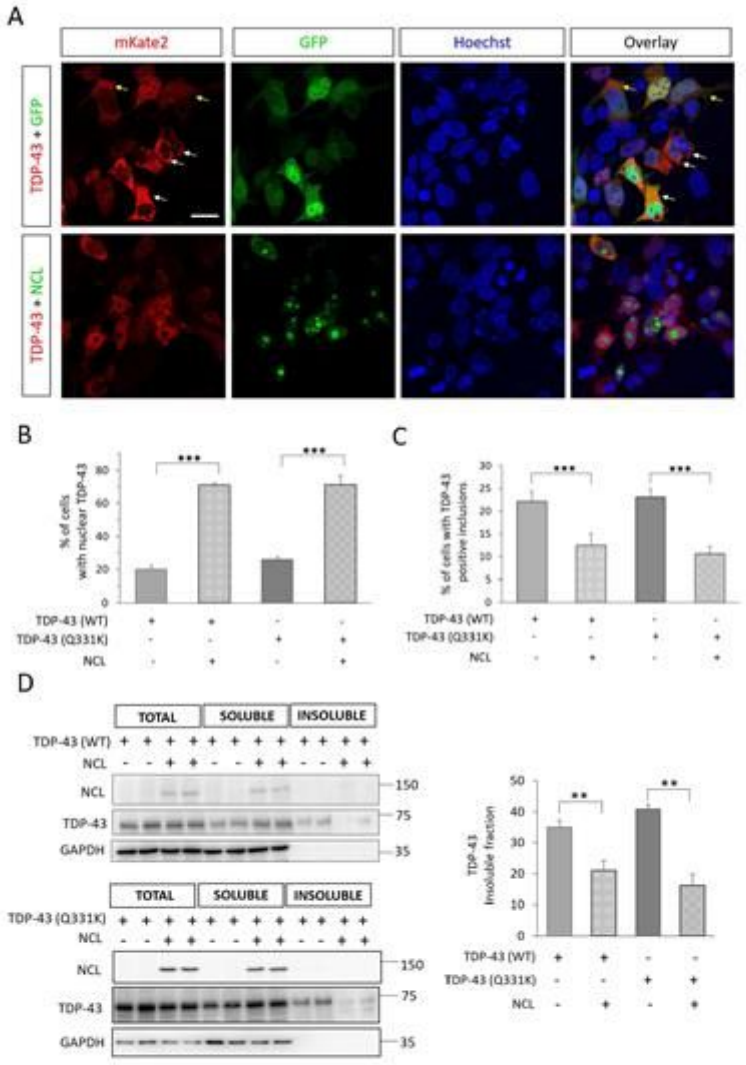

Figure 2

Increasing amount of TDP-43 is associated with increased levels of detergent insoluble TDP-43 fraction. A. After TDP-43 induction in galactose-containing liquid medium (6 h) in the different generated yeast strains, cells were observed by epifluorescence microscopy (right panels) to visualize the expression of

the TDP-43-GFP fusion protein. Images indicate that TDP-43-GFP chimeric construct in all strains (TDP 1C, TDP 2C, TDP 3C and TDP MC) localized into GFP-positive inclusions, which were different in both the number and size with no obvious correlation with the amount of expressed TDP-43. For each fluorescence image, differential interference contrast (DIC) micrographs are also reported (left panels). Shown images are representative of 3 biological replicates for each strain. Scale bar, 10 μm. B. Cell lysates (in a RIPA buffer) from different yeast strains harbouring increasing copies of the TDP-43-GFP transgene, grown in galactose-containing medium for 6 h to induce TDP-43 expression, were subjected to biochemical separation of detergent-soluble and -insoluble protein fractions as described in STAR Methods. Total, soluble and insoluble fractions (in a 1:1:1 ratio) were then analysed by WB for the presence of TDP-43. The upper panel reports representative WBs in which the presence of glyceraldehyde 3-phosphate dehydrogenase (GAPDH) was also analysed as a control for detergent-soluble proteins, indicating that the detergent-insoluble fraction of the TDP-43-GFP chimera (visible as a double band between 60 and 75 kDa) significantly increases in strains expressing the protein from two or more copies (2C, 3C, MC) of the transgene compared to the TDP 1C strain. This is better appreciable in the bar diagram of the lower panel, in which the densitometric quantification of TDP-43 immunoreactive bands is reported as the percentage ratio of the TDP-43 band intensity in each (soluble and insoluble) fraction over the sum of the band intensity in both fractions. All results represent mean band signal ± SEM. n=3, *p<0.05, **p<0.01, unpaired two-tailed Student's t-test for TDP 2C, TDP 3C and TDP MC compared to TDP 1C.

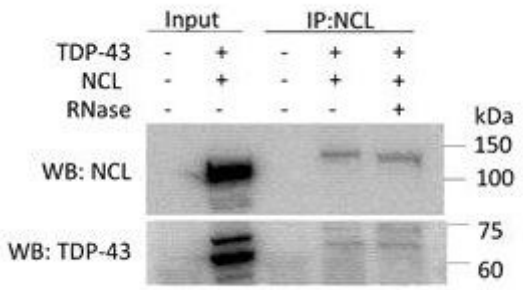

Figure 3

Both non-toxic and toxic TDP-43 expression levels alter yeast cell morphology from rounded to elongated phenotype. A. Control (CENPK), TDP 1C or TDP 2C strains were cultured in galactose-containing plates for 2 days to induce the expression of TDP-43-GFP. Cells were then fixed and analysed by DIC (for cell morphology, left panel) and epifluorescence (for TDP-43-GFP expression, right panel) microscopy. An aberrant elongated shape in both TDP 1C and TDP 2C cells is already appreciable by visual inspection. Shown images are representative of 3 biological replicates for each strain. Scale bar, 10 μm. B. A quantitative morphometric evaluation of cells, performed by calculating the ratio between the cell major and minor axes (taken as an approximation of cell ellipticity) from DIC micrographs, further supported a significant aberrant elongation (with a ≥60% increase of ellipticity) of TDP-43-expressing cells compared to the parental strain (CENPK). All results represent mean ± SEM. The number of biological replicates of

CENPK, TDP 1C and TDP2C is 6, 7, 8, respectively (with each replicate representing the mean value from 60-80 cells). **p<0.01, Kruskal-Wallis test followed by a Dunn's post hoc test.

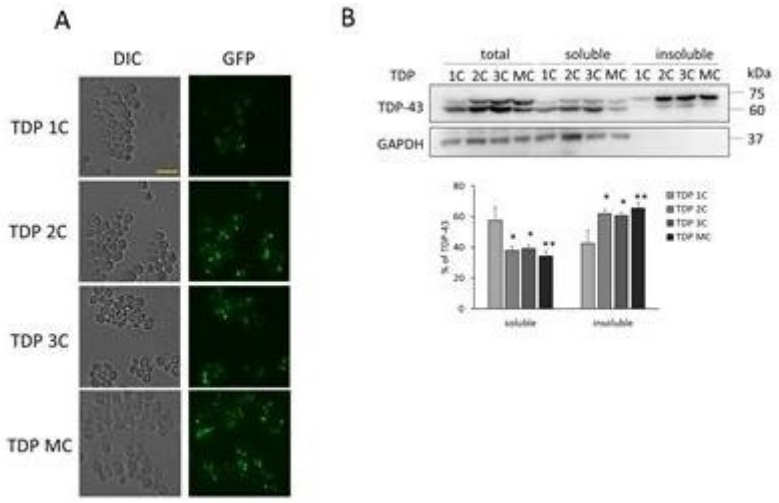

Figure 4

Two different ALS-associated mutations do not modify the TDP-43(WT)-induced phenotypes in yeast. A. The viability of S. cerevisiae strains expressing two chromosomally integrated copies of the ALS-associated M337V or Q331K missense mutants of human TDP-43 (as GFP-fused proteins) was compared to that of unmodified CENPK cells or the TDP 2C strain (bearing two copies of wild-type TDP-43-GFP (WT)) by the spot test. Three ten-fold different serial dilutions of cells from the different strains were grown (30 °C, 3 days) in either glucose- or galactose-containing medium, repressing or promoting, respectively, the expression of the (WT or mutated) TDP-43-GFP constructs. Both TDP-43 mutants show comparable lethality with respect to the WT protein. Other experimental details are as in the legend to Fig. 1A. B. The cell growth rate in the (M337V) and (Q331K) TDP 2C strains (measured as described in the legend to Fig. 1B) was significantly reduced compared to the CENPK control. Such a growth impairment was similar to that exerted by (WT) TDP 2C. The test was performed as described previously in the legend to Fig. 1B. Reported data are mean ± SEM, n=9 biological replicates for each strain. ** p<0.01, Kruskal-Wallis test followed by a Dunn's post hoc test. C. Expression of the (M337V) or (Q331K) TDP-43 mutants by two integrated copies resulted in the same elongated cell shape observed in the (WT) TDP 2C strain as determined by quantitative morphometric evaluation (as described in the legend to Fig. 3B). n=8 biological replicates for each strain, * p<0.05, *** p<0.001 Kruskal-Wallis test followed by a Dunn's post hoc test.

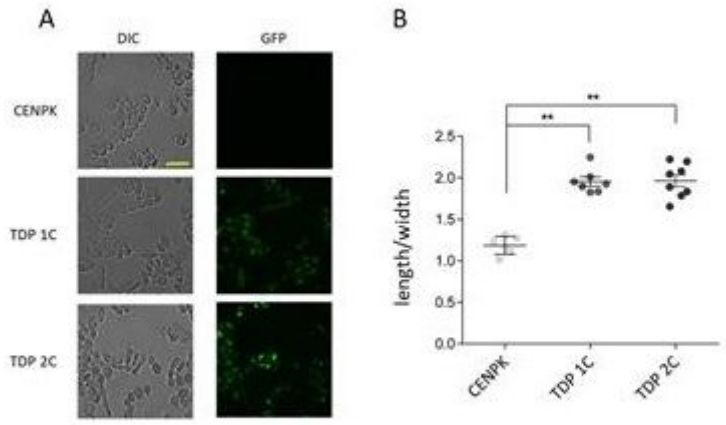

Figure 5

Overexpression of human NCL antagonizes the toxicity of WT and mutated TDP-43 in yeast. A. The growth of S. cerevisiae cells expressing two (2C) or three (3C) genomic copies of (GFP-fused) human TDP-43 (upper panel) or overexpressing the protein by a non-integrative multi-copy plasmid (MC) (lower panel) was analysed by the spot test (as described in Fig. 1A) in strains overexpressing (MC), or not (-), human nucleolin (NCL) as a fusion construct with the red fluorescent protein mKate-2 by a galactose inducible multi-copy plasmid. Images are representative of 3 experiments yielding comparable results. B. The cell growth rate of the yeast strains of panel A was also quantitatively determined as described in Fig. 1B. Reported data are mean ± SEM, n=9 biological replicates for each strains.**** $p<0.0001$ *** $p<0.001$, ** $p<0.01$, * $p<0.05$, Kruskal-Wallis test followed by a Dunn's post hoc test. Data from both panels A and B indicated that NCL counteracts TDP-43 cytotoxicity. C. The spot test (carried out as in panel A) showed that NCL is also able to rescue the cytotoxic phenotype induced by the expression of two integrated copies of the ALS-related mutants Q331K and M337V of TDP-43 .

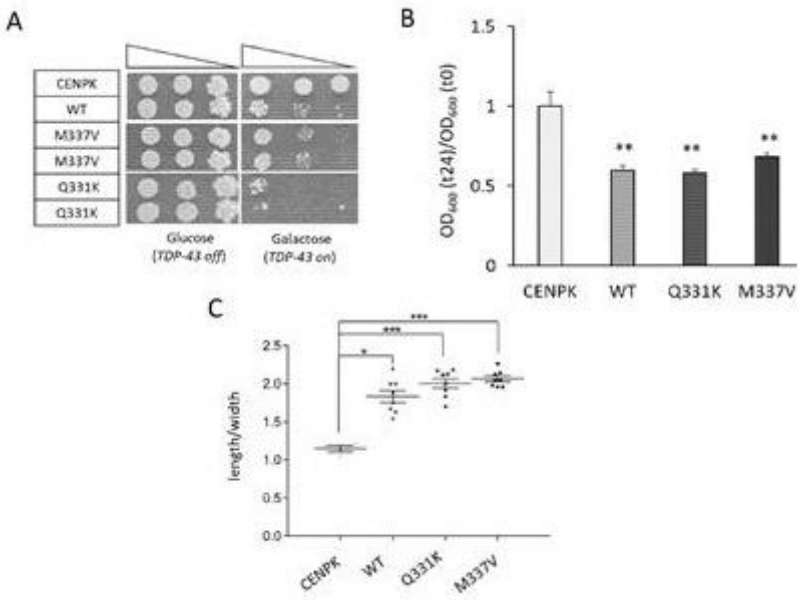

Figure 6

NCL overexpression reduced the detergent-insoluble TDP-43 fraction and reversed the altered cell shape due to the overexpression of TDP-43 in yeast. A. Cells from the TDP-43 2C strain (TDP 2C) transformed with a non-integrative multi-copy plasmid driving the over-expression of the NCL-mKate2 fusion protein (+/+), or mKate2 alone as control (+/-), respectively, were grown and analysed for the presence of detergent-soluble and -insoluble protein fractions in RIPA buffer lysates as described in the legend to Fig. 2B. In the upper panel, representative WBs for the presence of TDP-43, NCL and GAPDH (as a control for detergent-soluble proteins) in the total (TOTAL), detergent-soluble (S) and detergent-insoluble (I) protein fractions are shown. While GAPDH was always present in the soluble fraction only, and a small amount of NCL-mKate2 resulted insoluble, the amount of the TDP-43-GFP chimera partitioning in the insoluble fraction was substantially reduced by NCL overexpression. This is better described by the bar diagram of the lower panel reporting the densitometric quantification of TDP-43 immunoreactive bands, accomplished as described in the legend to Fig. 2B. Data are reported as mean ± SEM, n=5, ** $p<0.01$, unpaired two-tailed Student's t-test. B. The quantitative evaluation of cell shape carried out as described in the legend to Fig. 3B demonstrated that NCL overexpression was also able to rescue the morphologic phenotype observed in the TDP 2C strain (bearing two copies of the WT TDP transgene) transformed with the multicopy plasmid encoding mKate2 alone (WT/-). Indeed, the expression of the NCL-mKate2 (NCL) chimeric construct in the TDP 2C strain (WT/+) reduced the ellipticity index towards the values observed in the control CENPK strains expressing the NCL-mKate2 chimera (-/+) or mKate2 alone (-/-). NCL overexpression exerted similar effects also in the yeast strains bearing two chromosomal copies of the Q331K or M337V disease-associated mutants of TDP-43 (cfr. (Q/K)/- vs (Q/K)/+ and (M/V)/- vs (M/V)/+). Data are mean ± SEM. * $p<0.05$, ** $p<0.01$, **** $p<0.0001$, Kruskal-Wallis test followed by a Dunn's post hoc test (the number of the biological replicates for each condition being indicated in the bottom part of the panel). Other details are as in the legend to Figure 3B.

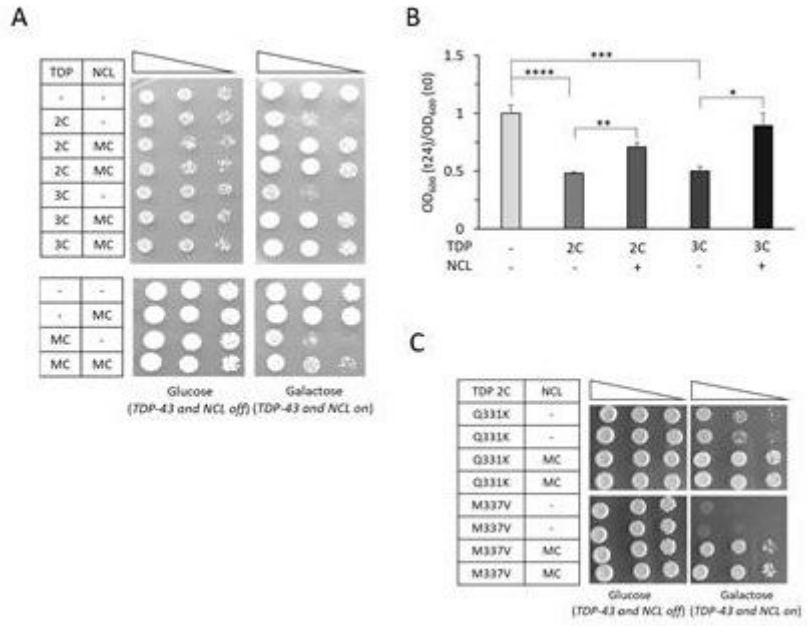

Figure 7

Proteomic analysis of TDP-43- and TDP-43/NCL-expressing yeast cells. A. Protein extracts from the yeast strain carrying one chromosomally integrated copy of the TDP-43-GFP transgene and the unmodified strain (CENPK) were subjected to a comparative tandem mass tag (TMT)-based proteomic study by mass spectrometry (MS). The 38 proteins whose expression levels were significantly altered in TDP-43-expressing cells above or below an arbitrary cut-off value (i.e., TDP-43/CENPK ratio > 1.33 or < 0.77, for up-regulated and down-regulated proteins, respectively) were subjected to a protein interaction network analysis by the STRING software using default settings. Up-regulated and down-regulated proteins are represented as red or blue octagonal node, respectively, with colour intensity being representative of the value of the TDP-43/CENPK ratio (i.e., dark red and blue colours indicating a TDP-43/CENPK ratio > 1.50 or < 0.66, respectively, for a total of 21 proteins). The thickness of lines between the proteins indicate the strength of the evidence supporting the functional interactions between them (see STAR methods). The protein full names are reported in Supplemental Table 2. B. The 21 proteins found to be mostly deregulated in the TDP 1C strain by the untargeted TMT proteomic approach were subjected to a parallel reaction monitoring (PRM)-based validation study in both the TDP 1C (light grey bars) and TDP 2C (dark grey) strains, compared to the control (CENPK) strain (black). Protein amounts are normalized to those measured in the CENPK strain. This analysis confirmed the deregulation of 20 out of the 21 chosen proteins (with the exception of AIM17) in the 2C strain (3 proteins), or both (1C and 2C) strains (16 proteins). C. The 20 proteins identified by the confirmation study of panel B were further subjected to a comparative PRM analysis in the TDP 1C and 2C strains in the absence or the presence of overexpressed NCL-mKate2. This analysis indicated that NCL significantly, increased the expression levels of 3 out of the 5 down-regulated proteins in the TDP 2C strain (ATP7, RDL1, YHI0). Protein amounts are normalized to those measured in the CENPK strain (dashed line). D. The analysis of panel C also showed that NCL

significantly decreased the expression of 5 out the 15 up-regulated proteins in the TDP 1C strain (HSP26, PRX1, AMPL, HFA1, CPYI), 2 proteins in the TDP 2C strain (HSP74, PGM2) and 1 protein in both strains (HSP82). Protein amounts are normalized to those measured in the CENPK strain (dashed line). The above proteomic analysis was carried out on 9 biological replicates for each strain. In panels B-D, data are reported as mean ± SEM; * p<0.05; # p<0.01, Student's t test.

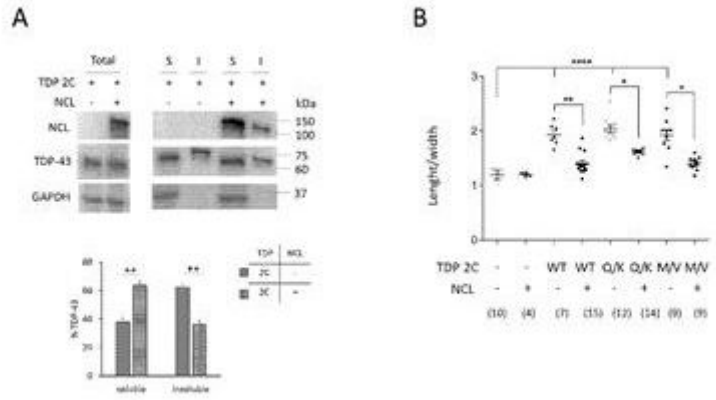

Figure 8

An extra-nuclear NCL fraction is probably responsible for the rescue of TDP-43 toxicity. A. The viability of S. cerevisiae (CENPK) strains either unmodified (-), or expressing the TDP-43-GFP construct (TDP) by two chromosomal copies (2C) and/or the NCL-mKate2 construct, containing either WT NCL or a deletion mutant of the protein lacking the nuclear localization signal (ΔNLS), by the multi-copy (MC) pYES2 plasmid was analysed by the spot test as described in the legend to Fig. 1A. The ΔNLS mutant of NCL had the same capacity to counteract the toxic TDP-43 phenotype as the WT. B. The viability spot test assay demonstrated that a construct in which NCL was fused to SV40 sequence (SV40-NCL), which causes the forced retention of the protein in the nucleus, completely lost the rescuing capability against TDP-43 noxious effect. All details are as in panel A.

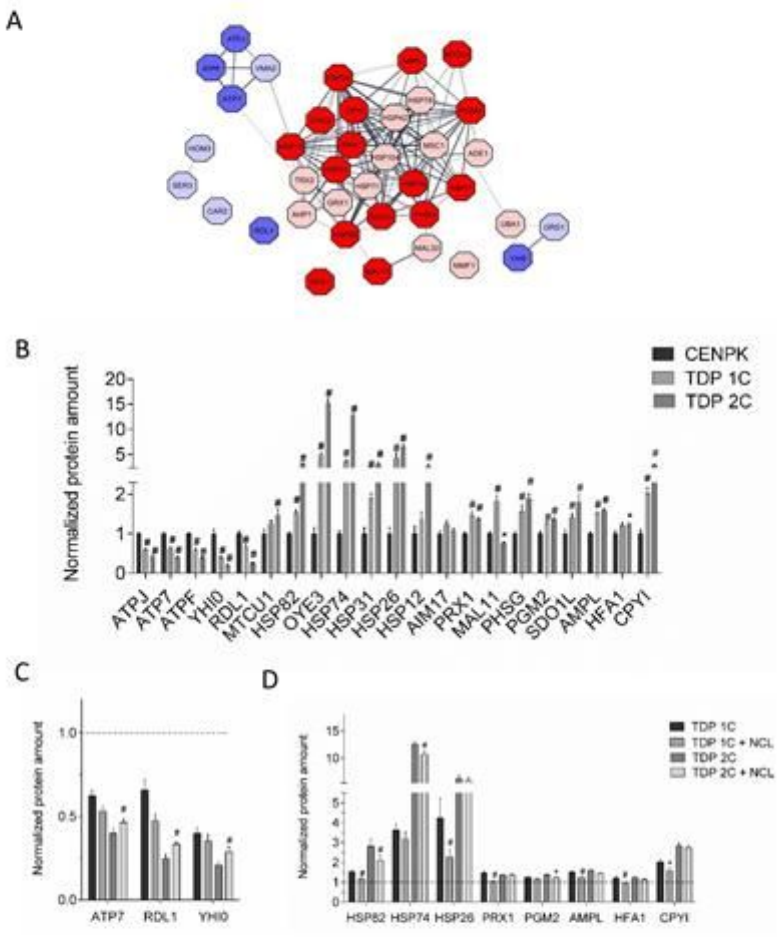

Figure 9

NCL rescues apoptosis induced by TDP-43 overexpression in human HEK293T cells. A. HEK293T cells were transiently co-transfected with plasmids coding for human TDP-43 (either WT or bearing the Q331K missense mutation) fused to mKate2 (TDP-43 (WT) and TDP-43 (Q331K), respectively) and human NCL fused to GFP (NCL) (+). As controls (-), cells were co-transfected with plasmids encoding mKate2 and/or GFP only. 48 h after transfection, cell viability was measured by the MTS assay, and data were normalized to the mean value of control samples (-/-/-). Both WT and Q331K TDP-43 consistently reduced (by ≈50%) cell viability compared to control cells, while co-expression of NCL significantly rescued such a toxic phenotype. NCL by itself did not affect cell viability (cfr. -/-/- and -/-/+ samples). Data are mean ± SEM, n=15 biological replicates for each strain, ** p<0.01, *** p<0.001 **** p<0.0001

Kruskal-Wallis test followed by a Dunn's post hoc test. B. Protein samples (20 µg) from lysates of HEK293T cells co-transfected as in panel A were resolved by SDS-PAGE, electroblotted onto PVDF membranes and probed with antibodies to GFP (recognizing the NCL-GFP chimera), TDP-43, the anti-apoptotic factor Bcl-2, and procaspase-3 and -9. The left panel shows a representative WB out of 4 biological replicates (i.e. different cell transfections) also showing the Coomassie blue staining of the membrane; the right panel reports the densitometric analysis of immunoreactive bands for Bcl-2, procaspase-3 and procaspase-9 in the different cell samples normalized to the optical density of the corresponding Coomassie blue-stained lane. The expression levels of the three analysed apoptosis markers are significantly decreased in HEK293T cells expressing the TDP-43 (either WT or Q331K) constructs (cfr. -/-/- and +/-/- or -/+/-), and partially or fully rescued upon co-expression of NCL-GFP (cfr. +/-/- and +/-/+, or -/+/- and -/+/+). Data are mean ± SEM, n=4; * p <0.05 ** p<0.001, Student's t test.

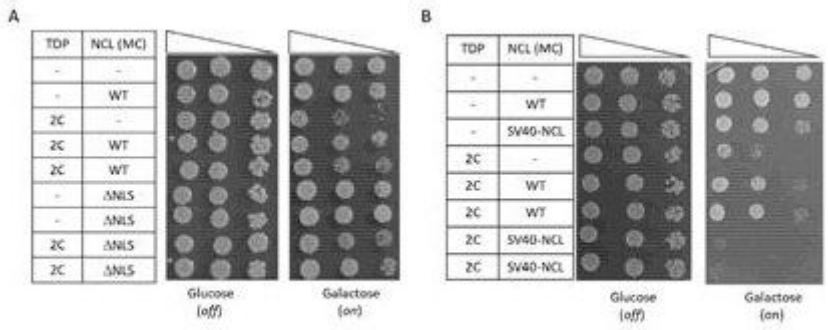

Figure 10

NCL rescued the nuclear localization of TDP-43, and reduced cytosolic inclusions and the detergent-insoluble fraction of TDP-43 in HEK293T cells. A- HEK293T cells transiently co-transfected with plasmids coding for human WT TDP-43 fused to mKate2 and either GFP alone (TDP-43 + GFP, upper panels), or the NCL-GFP chimera (TDP-43 + NCL, lower panels), were fixed, counterstained with the nuclear marker Hoechst 33342, and observed by confocal microscopy for the intracellular distribution of the different fluorescent proteins. The reported micrographs, representative of 3 biological replicates, show cells with nuclear (orange arrows) or uniform cytosolic (yellow arrows) localization of TDP-43-mKate2, or intense discrete cytosolic red signals suggestive of the presence of TDP-43-mKate2 aggregates (white arrows). Co-expression of NCL-GFP significantly reduced the presence of cells with aberrant extra-nuclear TDP-43-mKate2 localization. B- The bar diagram reports the percentage of cells co-expressing the TDP-43 (either WT or bearing the Q331K mutation)-mKate2 chimera and GFP (-) or NCL-GFP (+) having an exclusively nuclear mKate2 signal, with respect to the total of cells co-expressing both proteins. Such a value increased from ≅20-25% in TDP-43-mKate2/GFP co-transfected cells to ≅70% in TDP-43-mKate2/NCL-GFP co-transfected cells for both WT and Q331K TDP-43, suggesting that NCL was able to preserve the correct nuclear localization of TDP-43. For such quantitative analysis, 6 different fields from each biological replicate were considered. Data are mean ± SEM, n=3 (biological replicates); *** p<0.0005, Student's t test. C- The bar diagram reports the percentage of cell co-expressing either the WT or the Q331K mutant of TDP-43-mKate2 chimera and GFP (-) or NCL-GFP (+), presenting discrete (cytosolic)

aggregation-like foci, with respect to the total of cells co-expressing both proteins. Such a value significantly decreased by ≈50% in cells co-expressing NCL-GFP, suggesting that NCL was able to prevent aberrant cytosolic TDP-43 aggregation. For such quantitative analysis, 6 different fields from each biological replicate were considered. Data are mean ± SEM, n=3; *** p<0.0005, Student's t test. D-HEK293T cells transiently co-transfected with plasmids coding for human TDP-43 (either WT or carrying the Q331K mutation) fused to mKate2 and either GFP alone (+/-), or the NCL-GFP chimera (+/+), were lysed in RIPA buffer and subjected to separation of detergent-soluble and -insoluble fractions by ultracentrifugation. The left panels show representative WBs for the presence of NCL-GFP (with anti-GFP antibody), TDP-43-mKate2 (with anti-TDP-43 antibody) and GAPDH (as a control for detergent-soluble proteins) in total lysates (TOTAL), and detergent-soluble (SOLUBLE) and -insoluble (INSOLUBLE) protein fractions. WBs for WT and Q331K TDP-43 are reported in the upper and the lower part of the panel, respectively. The right panel, reporting the densitometric analysis of TDP-43-mKate2 immunoreactive bands as the percentage ratio between the insoluble fraction and the sum of the soluble and insoluble fractions (see also the legend to Fig. 2B), clearly shows that NCL overexpression significantly reduced the detergent insoluble amount of both WT and Q331K TDP-43 chimera (from ≈35% to ≈20%). GAPDH is found in the soluble fraction only, thus confirming the reliability of the fractionation protocol. Data are mean ± SEM, n=5 for TDP-43(WT), n=3 for TDP-43(Q331K); * p <0.05, ** p<0.001, Student's t test.

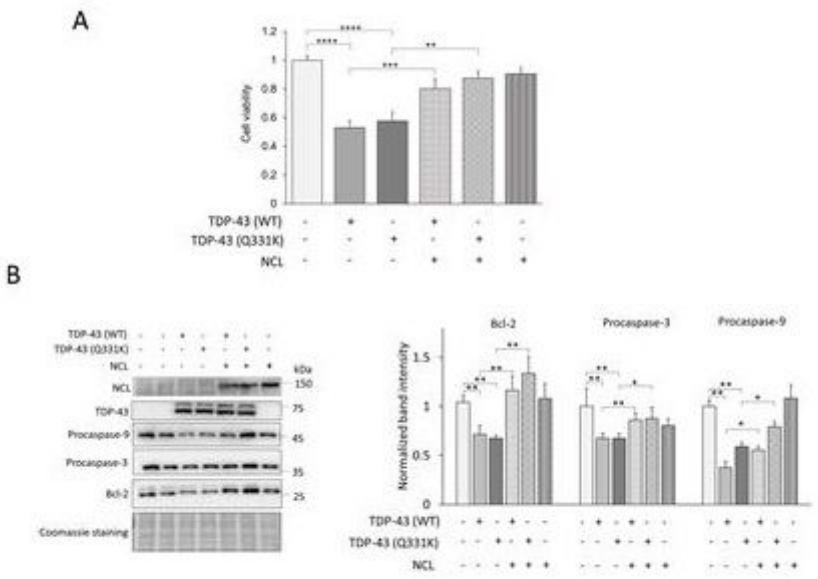

Figure 11

TDP-43-mKate2 and NCL-GFP co-immunoprecipitate in HEK293T cells. Lysates of HEK293T transiently co-transfected with constructs coding for TDP-43-mKate2 and NCL-GFP (+/+) and control non-transfected cells (-/-) were treated (+) or not (-) with RNase A and then subjected to immunoprecipitation using an anti-NCL antibody. The immunoprecipitated fraction was subjected to WB analysis using either anti-GFP (recognizing the NCL-GFP chimera, upper panel) or anti-TDP-43 (lower panels) antibodies, showing the presence of both NCL-GFP (band between 100 and 150 kDa) and TDP-43-GFP (bands

between 60 and 75 kDa) irrespective of RNase treatment. Fractions of the total lysate (Input) were analysed as controls. Shown data, representative of 3 different experiments providing comparable results, support the physical interaction between the two chimeric proteins in human cells and suggest that such an interaction is not mediated by RNA.

Supplementary Files

This is a list of supplementary files associated with this preprint. Click to download.

- Peggionetal.2020Supplementalinformation.pdf